

On a Nanoscopically-Informed Shell Theory of Single-Wall Carbon Nanotubes

Chandrajit Bajaj⁽¹⁾ Antonino Favata⁽²⁾ Paolo Podio-Guidugli⁽²⁾

⁽¹⁾Center for Computational Visualization, Institute for Computational Engineering and Sciences The University of Texas at Austin¹

⁽²⁾Dipartimento di Ingegneria Civile, Università di Roma Tor Vergata²

Abstract

This paper proposes a bottom-up sequence of modeling steps leading to a nanoscopically informed continuum, and as such macroscopic, theory of single-walled carbon nanotubes (SWCNTs). We provide a description of the geometry of the two most representative types of SWCNTs, armchair (A-) and zigzag (Z-), of their modules and of their elementary bond units. We believe ours to be the simplest shell theory that accounts accurately for the linearly elastic response of both A- and Z- CNTs. In fact, our theory can be shown to fit SWCNTs of whatever chirality; its main novel feature is perhaps the proposition of chirality-dependent concepts of effective thickness and effective radius.

PACS: 61.46.Fg, 62.25.-g, 46.70.De

Contents

1	Introduction	2
2	Nanoscale Energies	4
3	The Geometry of SWCNTs, from A to Z	5
3.1	Module and bond unit of an ACNT	6
3.2	Module and bond unit of a ZCNT	9

¹201 East 24th Street, Austin, TX 78712, USA

Email: bajaj@ices.utexas.edu

²Via Politecnico 1, 00133 Rome, Italy.

Email: favata@ing.uniroma2.it (A. Favata)

ppeg@uniroma2.it (P. Podio-Guidugli)

4	Nanoscale DSM. Axisymmetric Equilibrium Problems	11
4.1	Axial traction of an ACNT	11
4.2	Axial traction of a ZCNT	14
4.3	Torsion of an ACNT	16
4.4	Radial loading of an ACNT	19
4.5	Radial loading of a ZCNT	20
4.6	Energetics	22
4.6.1	The energy stored in A- and Z- CNTs under axial traction	22
4.6.2	The energy stored in a twisted armchair CNT	22
4.6.3	The energy stored in A- and Z- CNTs subject to radial loading	22
4.7	Slenderness and thinness	23
5	Nanoscale CSM. A SWCNT-Oriented Shell Theory	24
5.1	Displacement and strains	24
5.2	Constitutive parameters	26
5.3	Axisymmetric equilibria	26
5.3.1	Axial Traction	26
5.3.2	Torsion	26
5.3.3	Radial pressure	27
6	The Effective Parameters of CNT-like Shells	27
6.1	‘Continuous’ parameters	28
6.2	‘Discrete’ parameters	29
6.3	Elastic moduli, thickness, and radius, of CNT-like shells	31
7	Conclusions	35
8	Appendix. Ancillary Computations	37
8.1	Computations relative to Section 4.1	37
8.2	Computations relative to Section 4.2	39
8.3	Computations relative to Section 4.3	40
8.4	Computations relative to Section 4.4	41
8.5	Computations relative to Section 4.5	42
8.6	Computations relative to Section 6.2	42

1 Introduction

Carbon has a large variety of allotropic forms, natural and artificial: graphite, diamond, fullerene, carbon fibers, carbon nanotubes (CNTs), and others. The relative C-C bond complexes, diverse as they are by spatial dimensions and geometry, correspond to diverse hybrid electron states, made possible by combination of the electrons occupying the most external shells in a C atom; the nature and the strength of its C-C bond complex decide the mechanical properties of a given allotrope at any scale.

This paper proposes a bottom-up sequence of modeling steps leading to a nanoscopically informed continuum, and as such macroscopic, theory of single-walled carbon nanotubes (SWCNTs). Recently, modeling procedures of the same type have been adopted by various authors [15, 4, 24, 19, 20, 5, 28], with application to CNTs and polymer composites in mind. Related multiscale modeling papers, such as [1] and [16], cover a variety of tools for studying both quantum and classical models of atomic systems in crystalline phase, and propose techniques to connect the microscopic models to the continuum limits. They suggest that, for non-periodic systems, the key challenge lies in carefully defining average energy at the microscopic level and connecting it to a macroscopic energy. Another related paper is [18], that studies the mechanics of materials with periodic micro-structures; here, lattice structures are divided into two classes: truss materials modeled as beams with axial and bending stiffness, and frame materials modeled with pin-joints at the nodes.

There are of course differences in concept ingredients and developments in the cited papers, but their goal is one and the same: *to deduce the targeted macroscopic mechanical behavior from the available nanoscopic chemical-physical information*. In our present paper, a bridge between the nanoscopic and the macroscopic viewpoints is created by means of an intermediate passage, that we term *meta-nanoscopic*, in a fashion that we now describe. At the nanoscopic scale, the bonding and non-bonding energies keeping CNTs together are evaluated in the fashion of molecular mechanics (MM) (Section 2). In the following section, a mechanical caricature of a SWCNT as an orderly arrangement of pin-jointed sticks and (axial and spiral) springs is drawn, within the framework of discrete structure mechanics (DSM). This requires a preliminary careful description of the geometry of the two most representative types of SWCNTs, armchair (A-) and zigzag (Z-), of their modules and of their elementary bond units; in such description, the nanoscopic parameters are the chirality index and the length of the C-C bond. The viewpoints of MM and DSM are connected by equating the energies per bond, for each of which an approximate quadratic expression is accepted: two types of bonding energies – hence two purely constitutive parameters, the stiffness constants of the two types of springs – enter the expression for the DSM energy of a bond unit; they are taken equal to the two corresponding nanoscopic stiffness parameters, regarded as a known input from MM. This simple measure opens the way to the posing and solving, within the framework of DSM, of a number of equilibrium problems for SWCNTs (Section 4).

The step from discrete to continuous structure mechanics (CSM) is harder. To take it, a DSM model of SWCNT has to be assimilated to a suitable model taken from the library of CSM. The main difficulty in doing so resides in the number and nature of the parameters needed to specify a CSM model: no matter what rod or shell theory one chooses, the relative stiffness notion consists of a list of more than two combinations of both *constitutive* and *geometric* parameters, the latter reflecting theory-specific concepts of *thinness* and *slenderness*. Now, while there is a natural nanoscopic notion of slenderness for SWCNTs, to assess their thinness is a controversial issue, because a preliminary estimate of their

effective thickness is required (these matters are dealt with in Section 4.7); and, no doubt both slenderness and thinness of a SWCNT depend on its chirality. Therefore, one is faced with the problem of determining the chirality-dependent parameters of the continuum theory of his choice in terms of only two nanoscopic constitutive parameters and in the absence of an unequivocal nanoscopic concept of thinness.

For reasons that are discussed at length in [8] and recapitulated in Section 5, the CSM theory we adopt is a *linearly elastic theory of orthotropic shells*, where the independent constitutive parameters are four and the geometric parameters two. To determine all those parameters, firstly we solve the system of equilibrium equations ruling the *axial-traction* and *radial-loading* DSM problems for both A- and Z- CNTs, and the *torsion* problem for ACNTs (Sections 4.1–4.5); interestingly, the solutions we find hold for whatever slenderness. Secondly, we import from [8] the analytic solutions there found for the same equilibrium problems, when set within the framework of the above mentioned shell theory. While the torsion solution is insensitive to slenderness, the axial-traction and radial-loading solutions are; for simplicity, we confine attention to the case of slender shells. Thirdly, for each of these boundary-value problems, both in the discrete and in the continuous formulation, we regard the involved nanotubes as cylindrical *probes*, whose relevant stiffnesses and Poisson-like contraction ratios we define in the fashion of standard rod theory (Sections 6.1 and 6.2, respectively). Finally, in Section 6.3, the sought-for parameters are found by equating the continuous and discrete stiffnesses and contraction ratios; since we have an unusually rich crop of solutions at our disposal, this can be done in more than one way, with convincingly consistent results.

We believe ours to be the simplest shell theory that accounts accurately for the elastic response of both A- and Z- CNTs. In fact, modulo a modest generalization to be presented elsewhere, our theory can be shown to fit SWCNTs of whatever chirality; its main novel feature is perhaps the proposition of chirality-dependent concepts of effective thickness and effective radius; for a discussion of this issue, and others, we refer the reader to our conclusion section.

2 Nanoscale Energies

At nanometer scale, atomic interactions are modeled by either quantum mechanics (QM) or molecular mechanics (MM), in both cases by striving to capture how and to what extent the system’s energy varies with changes in atomic positions. QM can describe rigorously the electronic structure of a material complex, but its computational cost quickly becomes prohibitive as the number of atoms involved increases. MM is based on the *Born–Oppenheimer approximation* for the Hamiltonian of a collection of heavy and light particles, a cornerstone of computer simulations. Consistent with this simplifying assumption, the total energy U of such a material complex is expressed as a sum of two terms:

$$U = U_b + U_{nb},$$

where U_b and U_{nb} , denote, respectively, the *bonding energies* and the *non-bonding energies*. The latter account for van der Waals and Coulomb interactions. However, when modeling SWCNT, the contribution of Coulomb interactions is usually neglected since interactions are predominantly between essentially neutral carbon atoms. Within the same modeling context, the former consist of four parts:

$$U_b = U_\rho + U_\theta + U_\omega + U_\tau,$$

where $U_\rho, U_\theta, U_\omega$ and U_τ denote the energies respectively associated with *stretching* (of a covalent bond), *angle variation* (between two covalent bonds), *torsion* (around bonds), and the so-called *improper torsion* (see e.g. [19]). The third and fourth contributions are considered negligible when compared with U_ρ and U_θ , whose harmonic approximations are:

$$U_\rho = \frac{1}{2} \sum k_\rho (\rho - \rho^{\text{ref}})^2,$$

$$U_\theta = \frac{1}{2} \sum k_\theta (\theta - \theta^{\text{ref}})^2.$$

Thus, the only bond-stiffness constants of importance are k_ρ and k_θ ; they can be obtained by *ab initio* QM evaluations or fitted to experiments. The values we shall employ in our numerical computations,

$$k_\rho = 742 \text{ nN/nm} \quad \text{and} \quad k_\theta = 1.142 \text{ nN} \times \text{nm},$$

are the same as in [4] and [24].

3 The Geometry of SWCNTs, from A to Z

CNTs were discovered in 1991 by S. Iijima [12]. They look like right cylinders with approximately emispherical caps due to the actual manufacturing procedures, and can be single- or multi-wall. In imagination, SWCNTs can be obtained by rolling up into a cylindrical shape a *graphene*, that is, a monolayer flat sheet of graphite that can be visualized as a two-dimensional lattice with hexagonal unit cell. There are many ways to roll a graphene up, sorted by introducing a geometrical object, the *chiral vector*:

$$\boldsymbol{\chi} = n\mathbf{a}_1 + m\mathbf{a}_2$$

(Fig. 1). Having fixed \mathbf{a}_1 and \mathbf{a}_2 , the pairs of integers (n, m) specifies the chirality of a CNT; $(n, 0)$ - and (n, n) -nanotubes are called, respectively, *zigzag* and *armchair* (Fig. 2; roll-up axes are chosen perpendicular to chiral axes).³

Chirality influences all geometrical and mechanical properties of a CNT; for example, the radius of the cylinder on which a (n, m) -SWNT sits is:

$$\rho_0 = \hat{\rho}_0(n, m) := \frac{1}{2\pi} \sqrt{3(n^2 + nm + m^2)} s, \quad (1)$$

³The *chiral angle* is defined to be $\hat{\chi}(n, m) = \arctan(\sqrt{3}\frac{m}{m+2n})$; thus, in particular, the chiral angle of an armchair CNT is $\pi/6$ radians.

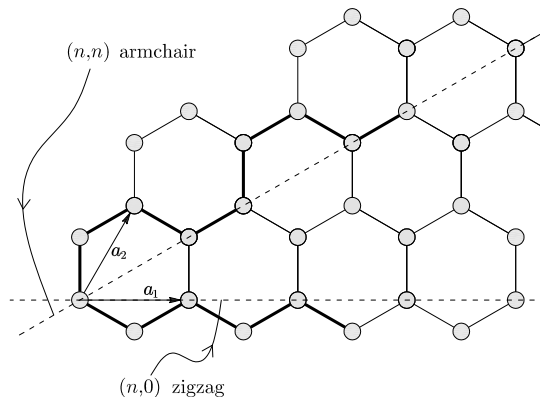


Figure 1: Graphene and its zigzag and armchair chiral axes.

where s the side length of a graphene cell; and, chirality influences the effective extension and shear moduli and the buckling strain [2, 3, 7, 23, 31]; needless to say, for multi-wall carbon nanotubes (MWCNTs), the chirality of the inner walls is hard to inspect.

In this paper, we concentrate on SWCNTs, armchair and zigzag; for short, we designate them by ACNTs and ZCNTs, respectively. The geometry of their undeformed reference configurations is described just below. To get acquainted with their size, it is convenient to start from a graphene cell: its side length s equals the C–C bond length, about 0.142 nm (that is, roughly, the diameter of a C atom); consequently, two opposite C atoms are spaced by $(1 + 2 \cos \pi/3)s = 0.283$ nm = the cell’s diameter; and, equally placed C atoms belonging to adjacent cells are spaced by $|\mathbf{a}_1| = |\mathbf{a}_2| = (2 \sin \pi/3)s = 0.2456$ nm, the distance of two parallel sides of a cell (to fix ideas, the spacing between two adjacent cylinders in a MWNT is about 0.34 nm).

3.1 Module and bond unit of an ACNT

Figure 3 is an atom-and-bond cartoon of the module of the ACNT having the smallest radius one can think of ($n = 2$), in its reference configuration. Whatever n , the *geometrically necessary radius*, that is, the radius of the cylinder on which the centers of the C atoms are placed, is:

$$\hat{\rho}_0(n, n) =: \rho_0^A(n) = \frac{3}{2\pi} n s \quad (2)$$

(cf. (22)); the total number of atoms per module is:

$$N^{AM} = 4 \times 2n = 8n.$$

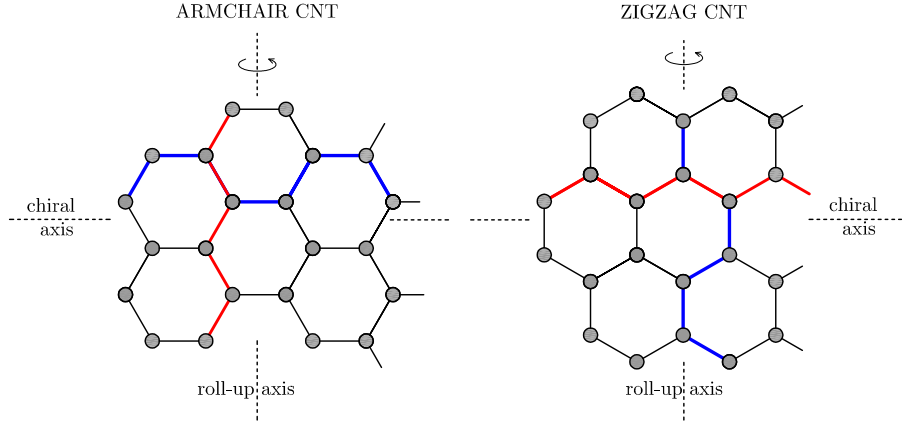


Figure 2: Graphenes to be rolled up into armchair (left) and zigzag (right) single-wall CNTs. Note the orthogonality of zigzag (red) and armchair (blue) atom sequences.

distinguish two types of sticks, a horizontal and b oblique, and two types of angles between sticks, denoted by α and β ; in a module, there are:

$$\begin{aligned}
 N_a^{AM} &= 4 \times n && \text{type } a \text{ sticks;} \\
 N_b^{AM} &= 4 \times 2n = 8n && \text{type } b \text{ sticks;} \\
 N_\alpha^{AM} &= 4 \times 2n = 8n && \text{type } \alpha \text{ angles;} \\
 N_\beta^{AM} &= 4 \times 4n = 16n && \text{type } \beta \text{ angles.}
 \end{aligned} \tag{3}$$

Three adjacent sticks, two of type b and one of type a , form an armchair bond unit (ABU). We make the geometry of an undeformed ABU precise with reference to Figures 4 and 5, where atom A is sitting at the origin of an orthogonal cartesian frame of unit vectors \mathbf{c}_i , with $\mathbf{c}_1 \equiv \mathbf{b}$. Note that

$$\cos \beta = -\cos \frac{\alpha}{2} \cos \gamma, \quad \gamma = \frac{\pi}{2n}, \tag{4}$$

and that the three next neighbors of A sit at the ends of the relative position vectors:

$$\begin{aligned}
 s^{-1} \mathbf{p}_B &:= \mathbf{b} = \mathbf{c}_1, \\
 s^{-1} \mathbf{p}_C &:= \mathbf{c} = \cos \frac{\alpha}{2} \mathbf{a} + \sin \frac{\alpha}{2} \mathbf{c}_3, \\
 s^{-1} \mathbf{p}_D &:= \mathbf{d} = \cos \frac{\alpha}{2} \mathbf{a} - \sin \frac{\alpha}{2} \mathbf{c}_3,
 \end{aligned} \tag{5}$$

where the unit vector

$$\mathbf{a} = -\cos \gamma \mathbf{c}_1 + \sin \gamma \mathbf{c}_2 \tag{6}$$

is orthogonal to \mathbf{c}_3 ; moreover,

$$\mathbf{e} = -\cos 2\gamma \mathbf{c}_1 + \sin 2\gamma \mathbf{c}_2. \tag{7}$$

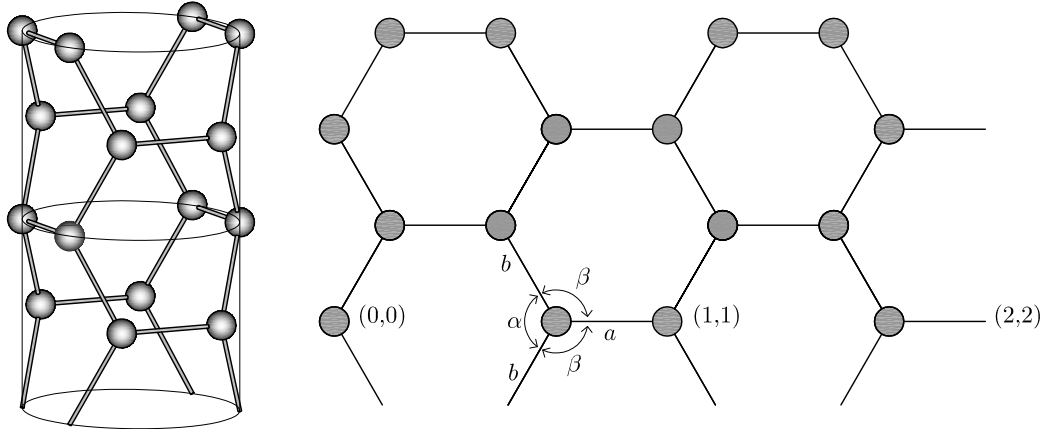


Figure 3: The module of a (2,2)-CNT, rolled and not.

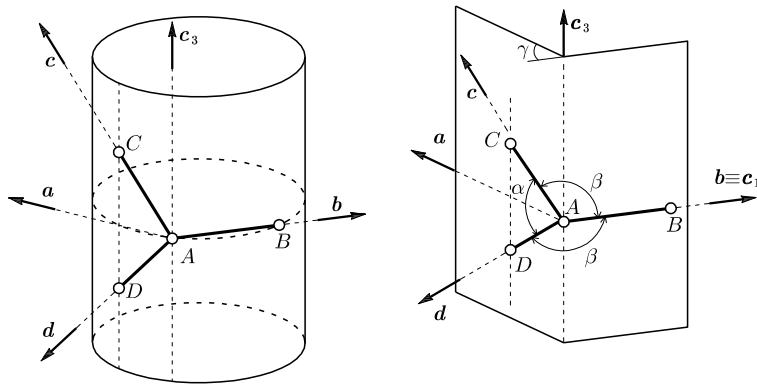


Figure 4: The geometry of an ABU: front view.

Remark. One may wonder why we have not set $\alpha = 2\pi/3$ in the formulas just above. This is in fact the case for the undeformed configuration, when we deduce from (4) that

$$\beta = \widehat{\beta}^A(n) = \pi - \arccos\left(\frac{1}{2} \cos \frac{\pi}{2n}\right). \quad (8)$$

Our reason is that (4)₁ holds also when the applied loads induce deformations that, while changing angles of both types α and β , do not change angle γ and preserve the mirror symmetry with respect to the plane through A orthogonal to \mathbf{c}_3 of the position vectors of atoms C and D (e.g., these conditions are met in the axial-traction problem we are going to study in Section 4.1, but they are not in the torsion problem studied in Section 4.3). We record here for later use an expression of $\Delta\beta$ as a function of $\Delta\alpha$ that follows by differentiation of (4)₁

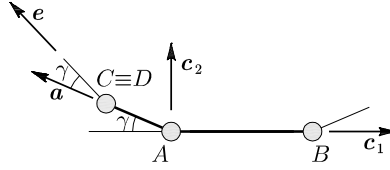


Figure 5: The geometry of an ABU: top-down view.

while keeping γ fixed:

$$\Delta\beta = -\widehat{\delta}^A(\alpha, \beta, \gamma)\Delta\alpha, \quad \widehat{\delta}^A(\alpha, \beta, \gamma) := \frac{\sin \frac{\alpha}{2}}{2 \sin \beta} \cos \gamma = \frac{\sqrt{3}}{4 \sin \beta} \cos \gamma. \quad (9)$$

(cf. eq. (14) of [4]).

3.2 Module and bond unit of a ZCNT

The module of a ZCNT of smallest radius ($n = 2$) is drawn in Figure 6; Figure 7 is relative to the cases $n = 4$ and $n = 10$. The cylinder's radius and the total

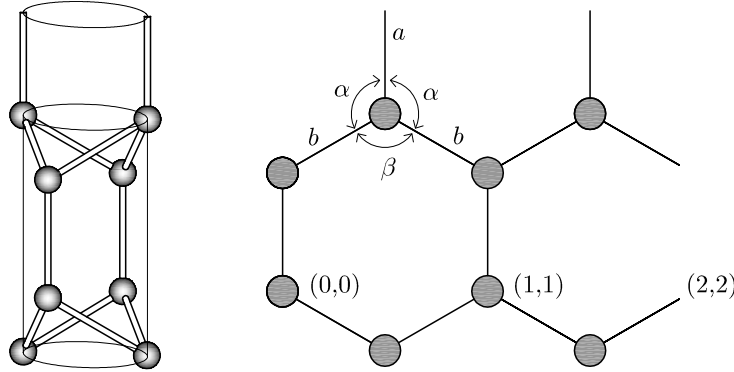


Figure 6: The module of a $(2,0)$ -CNT.

number of atoms per module are, respectively,

$$\widehat{\rho}_0(n, 0) =: \rho_0^Z(n) = \frac{\sqrt{3}}{2\pi} n s \quad \text{and} \quad N^{ZM} = 4 \times n = 4n. \quad (10)$$

In each module, there are:

$$\begin{aligned} N_a^{ZM} &= 2 \times n = 2n && \text{type } a \text{ sticks;} \\ N_b^{ZM} &= 2 \times 2n = 4n && \text{type } b \text{ sticks;} \\ N_\alpha^{ZM} &= 2 \times 4n = 8n && \text{type } \alpha \text{ angles;} \\ N_\beta^{ZM} &= 2 \times 2n = 4n && \text{type } \beta \text{ angles.} \end{aligned} \quad (11)$$

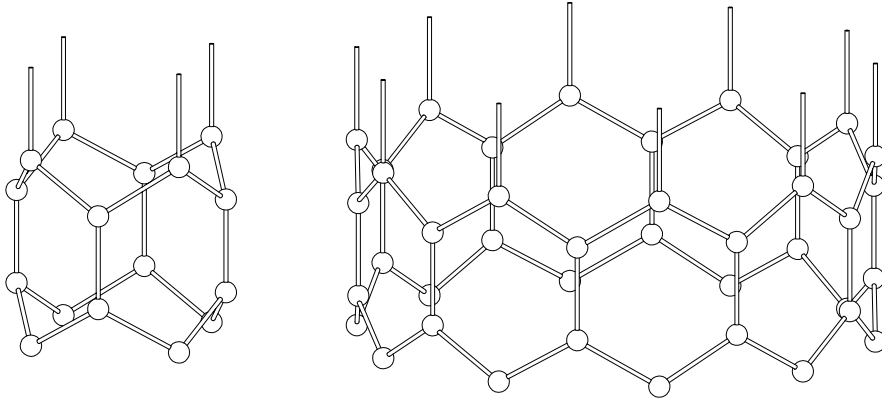


Figure 7: A (4,0)- and a (10,0)-CNT.

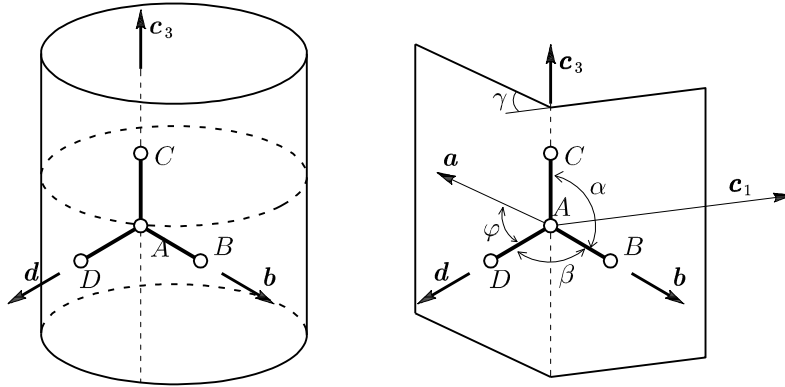


Figure 8: The geometry of a ZBU: front view.

Figures 8 and 9 illustrate a zigzag bond unit (ZBU) and its geometry. We see that the three next neighbors of the typical atom A , labeled B , C and D , sit at the following positions:

$$\begin{aligned}
 s^{-1}\mathbf{p}_B &:= \mathbf{b} = \cos \varphi \mathbf{c}_1 - \sin \varphi \mathbf{c}_3 \\
 s^{-1}\mathbf{p}_C &:= \mathbf{c}_3, \\
 s^{-1}\mathbf{p}_D &:= \mathbf{d} = \cos \varphi \mathbf{a} - \sin \varphi \mathbf{c}_3,
 \end{aligned} \tag{12}$$

with the unit vector \mathbf{a} as in (6); note that $\alpha = \varphi + \pi/2$. It is not difficult to show that angles α , β and γ are related as follows:

$$\cos \beta = \cos^2 \alpha - \sin^2 \alpha \cos \gamma, \tag{13}$$

whence

$$\beta = \widehat{\beta}^Z(n) = \arccos \left(\frac{1}{4} - \frac{3}{4} \cos \frac{\pi}{n} \right). \tag{14}$$

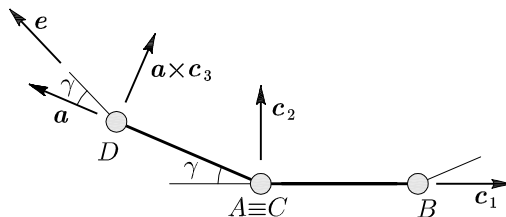


Figure 9: The geometry of a ZBU: top-down view.

On repeating the considerations proposed in Remark 1, and under the same circumstances, differentiation of (13) yields:

$$\Delta\beta = \widehat{\delta}^Z(\alpha, \beta, \gamma)\Delta\alpha, \quad \widehat{\delta}^Z(\alpha, \beta, \gamma) := \frac{\sin 2\alpha}{\sin \beta}(1 + \cos \gamma) = -\frac{\sqrt{3}}{2\sin \beta}(1 + \cos \gamma). \quad (15)$$

Remark. Here and henceforth, to lighten our notation, we write β in the place of $\widehat{\beta}^Z(n)$ and $\widehat{\beta}^A(n)$; no confusion should arise, because the type of nanotube we deal with is always clear from the context.

4 Nanoscopic DSM. Axisymmetric Equilibrium Problems

We view a meta-nanosopic mechanical model of a SWCNT as consisting of pin-jointed rigid sticks and linearly elastic springs, of two types: (1) *axial*, sensitive to changes in distance of the two C atoms sitting at the ends of the coaxial stick, of stiffness k_a ; (2) *spiral*, sensitive to changes in angle of the two sticks they are attached to, of stiffness k_a . Our mechanical model of an ABU looks as in Figure 10 (left); the zigzag case is shown in Figure 11 (left).

In this section we apply the principles and methods of DSM to solve explicitly a number of axisymmetric equilibrium problems for SWCNTs, namely, *axial traction and radial loading for both A- and Z- CNTs*, and *torsion for ACNTs*. Problem by problem, different symmetries are presumed that simplify considerably the solution process: to guess those symmetries correctly is at times not trivial; once they are detected, it is a matter of elementary vector algebra. For this reason, in each of the subsections here below, we relegate the ancillary computations to the Appendix.

4.1 Axial traction of an ACNT

This problem has been dealt with in [4, 15, 24], for zigzag CNTs as well. Figure 12 is meant to give a helping hand to visualize an ABU and its immediately adjacent sticks when, on applying Euler's *Cut Principle*, that ABU is required to be an equilibrated part of a nanotube subject to axial traction and, accordingly,

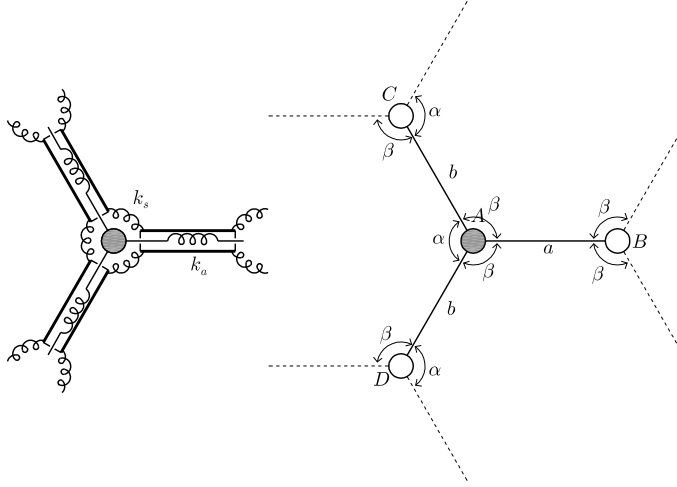


Figure 10: A stick-and-spring caricature of an ABU.

is regarded as acted upon by a balanced system of forces and couples, due to its interactions with the adjacent sticks. We assume that forces \mathbf{f}_B , \mathbf{f}_C , and \mathbf{f}_D , such that

$$\mathbf{f}_B + \mathbf{f}_C + \mathbf{f}_D = \mathbf{0}, \quad (16)$$

are applied at points B , C , and D . In view of the peculiar symmetries of the axial traction problem, we presume that

$$\begin{aligned} \mathbf{f}_B \cdot \mathbf{c}_3 &= 0, \\ \mathbf{f}_C \cdot \mathbf{c}_3 &= -\mathbf{f}_D \cdot \mathbf{c}_3, \\ \mathbf{f}_C \cdot \mathbf{c}_\alpha &= \mathbf{f}_D \cdot \mathbf{c}_\alpha = -\frac{1}{2} \mathbf{f}_B \cdot \mathbf{c}_\alpha \quad (\alpha = 1, 2) \end{aligned} \quad (17)$$

(note that, with these presumptions, (16) is satisfied).

In addition to forces, at both ends of each stick a number of couples are applied, which we distinguish into external and internal with reference to the Euler's cut which singled out the ABU. With a view toward writing moment balances, we stop and make our vectorial representation for couples unambiguous, with the help of Figure 13. The figure alludes to a linearly elastic spiral spring of stiffness k_s and rest angle ϑ , connecting two pin-jointed rigid sticks directed along the unit vectors \mathbf{u} , \mathbf{v} . When the angle changes by $|\Delta\vartheta|$, the spring exerts a couple

$$\boldsymbol{\tau} = \tau \mathbf{u} \times \mathbf{v}, \quad \tau = k_s \Delta\vartheta |\mathbf{u} \times \mathbf{v}|^{-1},$$

on the stick along \mathbf{u} and a couple $\boldsymbol{\tau} = -\tau \mathbf{u} \times \mathbf{v}$ on the other stick; thus, for $\Delta\vartheta < 0$, a clockwise (counterclockwise) couple is exerted on the stick along \mathbf{u} (\mathbf{v}). For example, upon loading the nanotube, the stick AC has external couples

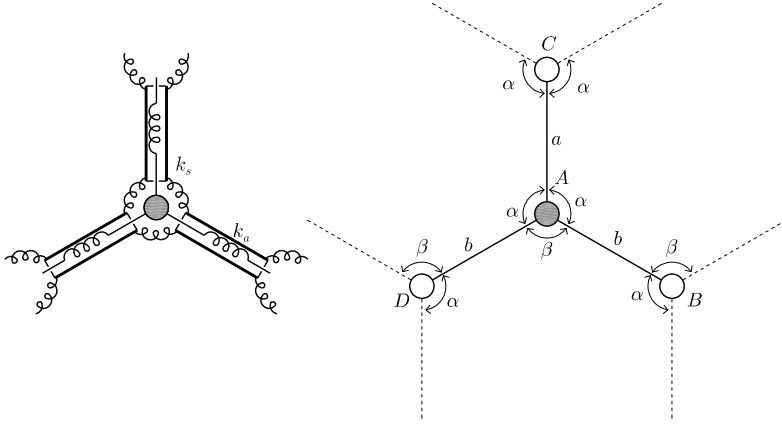


Figure 11: A stick-and-spring caricature of a ZBU.

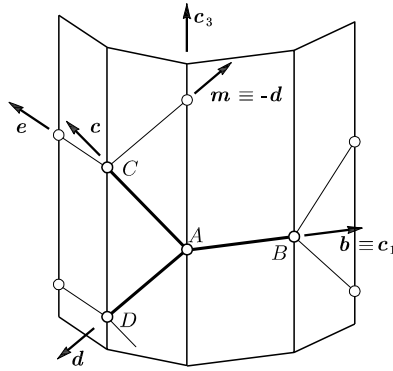


Figure 12: An ABU and its adjacent sticks.

$\bar{\tau}_\alpha, \bar{\tau}_\beta$ applied in C and internal couples τ_α, τ_β applied in A , with

$$\begin{aligned}\bar{\tau}_\alpha &= \bar{\tau}_\alpha (-\mathbf{c}) \times \mathbf{m}, \quad \bar{\tau}_\alpha = k_s \overline{\Delta\alpha} |\mathbf{c} \times \mathbf{m}|^{-1}, \\ \bar{\tau}_\beta &= -\bar{\tau}_\beta \mathbf{e} \times (-\mathbf{c}), \quad \bar{\tau}_\beta = k_s \overline{\Delta\beta} |\mathbf{e} \times \mathbf{c}|^{-1}\end{aligned}\tag{18}$$

and

$$\begin{aligned}\tau_\alpha &= \tau_\alpha \mathbf{c} \times \mathbf{d}, \quad \tau_\alpha = k_s \Delta\alpha |\mathbf{c} \times \mathbf{d}|^{-1}, \\ \tau_\beta &= -\tau_\beta \mathbf{b} \times \mathbf{c}, \quad \tau_\beta = k_s \Delta\beta |\mathbf{b} \times \mathbf{c}|^{-1}.\end{aligned}\tag{19}$$

With a further application of the Cut Principle, the moments of the force and couple system acting on stick AC are balanced with respect to the pole A if it so happens that

$$\mathbf{p}_C \times \mathbf{f}_C + \tau_\alpha + \tau_\beta + \bar{\tau}_\alpha + \bar{\tau}_\beta = \mathbf{0}\tag{20}$$

where we presume that

$$\overline{\Delta\alpha} = \Delta\alpha, \quad \overline{\Delta\beta} = \Delta\beta\tag{21}$$

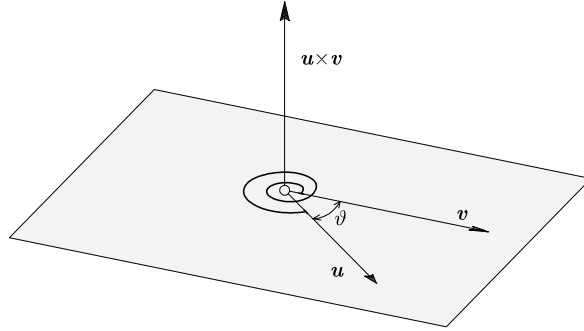


Figure 13: The couple associated with a spiral spring.

(the problem's symmetries exonerate us from laying down the relation for stick AD , which would not add any relevant information). Likewise, moments of force and couples system acting on stick AB are balanced with respect to A provided that

$$\mathbf{p}_B \times \mathbf{f}_B = \mathbf{0},$$

whence

$$\mathbf{f}_B \cdot \mathbf{c}_2 = 0. \quad (22)$$

Algebraic manipulations to be found in Section 8.1 lead us to conclude that the changes in length of sticks of type a and b are:

$$\Delta a = \frac{\mathbf{f}_B \cdot \mathbf{b}}{k_a} = 0, \quad \Delta b = \frac{\mathbf{f}_C \cdot \mathbf{c}}{k_a} = \sin \frac{\alpha}{2} f/k_a = \frac{\sqrt{3}}{2} f/k_a, \quad (23)$$

moreover, as to angle changes, we have:

$$\begin{aligned} \Delta \alpha &= \frac{1}{2} \cos \frac{\alpha}{2} \left(1 + \frac{1}{2} \left(\frac{\tan \frac{\alpha}{2}}{\tan \beta} \right)^2 \right)^{-1} f s/k_s = \frac{1}{4} \left(1 + \frac{3}{2 \tan^2 \beta} \right)^{-1} f s/k_s, \\ \Delta \beta &= \frac{\sin \frac{\alpha}{2}}{4 \tan \beta} \left(1 + \frac{1}{2} \left(\frac{\tan \frac{\alpha}{2}}{\tan \beta} \right)^2 \right)^{-1} f s/k_s = \frac{\sqrt{3}}{8 \tan \beta} \left(1 + \frac{3}{2 \tan^2 \beta} \right)^{-1} f s/k_s, \end{aligned} \quad (24)$$

where angle β depends on the chirality index n as specified by (8) (recall Remark 3.2).

4.2 Axial traction of a ZCNT

With reference to Figures 14 and 9, let a system of forces satisfying (16) be applied at points B, C , and D of a typical ZBU, singled out in Euler's manner to assess its equilibrium conditions as a part of a zigzag nanotube subject to

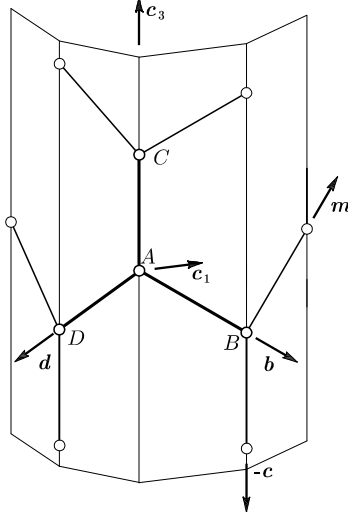


Figure 14: A ZBU and its adjacent sticks.

axial traction. The built-in symmetries require that:

$$\begin{aligned}
 \mathbf{f}_C &= f \mathbf{c}_3, \\
 \mathbf{f}_B \cdot \mathbf{c}_3 &= \mathbf{f}_D \cdot \mathbf{c}_3 = -\frac{1}{2} \mathbf{f}_C \cdot \mathbf{c}_3 = -\frac{1}{2} f, \\
 \mathbf{f}_D \cdot \mathbf{a} &= \mathbf{f}_B \cdot \mathbf{c}_1, \quad \mathbf{f}_D \cdot \mathbf{a} \times \mathbf{c}_3 = \mathbf{f}_B \cdot \mathbf{c}_2.
 \end{aligned} \tag{25}$$

As to moment equilibrium, that of stick AC with respect to A is automatic, given the symmetries. Not so for stick AB : it must be that

$$\mathbf{p}_B \times \mathbf{f}_B + \boldsymbol{\tau}_\alpha + \boldsymbol{\tau}_\beta + \bar{\boldsymbol{\tau}}_\alpha + \bar{\boldsymbol{\tau}}_\beta = \mathbf{0}, \tag{26}$$

where

$$\begin{aligned}
 \boldsymbol{\tau}_\alpha &= \tau_\alpha \mathbf{b} \times \mathbf{c}_3, \quad \tau_\alpha = k_s \Delta\alpha |\mathbf{b} \times \mathbf{c}_3| \\
 \bar{\boldsymbol{\tau}}_\alpha &= \bar{\tau}_\alpha (-\mathbf{b}) \times (-\mathbf{c}_3), \quad \bar{\tau}_\alpha = k_s \overline{\Delta\alpha} |\mathbf{b} \times \mathbf{c}_3| \\
 \boldsymbol{\tau}_\beta &= -\tau_\beta \mathbf{d} \times \mathbf{b}, \quad \tau_\beta = k_s \Delta\beta |\mathbf{d} \times \mathbf{b}|^{-1} \\
 \bar{\boldsymbol{\tau}}_\beta &= -\bar{\tau}_\beta \mathbf{m} \times (-\mathbf{b}), \quad \bar{\tau}_\beta = k_s \overline{\Delta\beta} |\mathbf{b} \times \mathbf{m}|^{-1}
 \end{aligned}$$

with \mathbf{b} , \mathbf{d} as in (12) and

$$\mathbf{m} = \sin \alpha (\cos \gamma \mathbf{c}_1 + \sin \gamma \mathbf{c}_2) - \cos \alpha \mathbf{c}_3.$$

Equation (26) reads:

$$\mathbf{b} \times \left(s \mathbf{f}_B + 2 \tau_\alpha \mathbf{c}_3 + \tau_\beta (\mathbf{d} - \mathbf{m}) \right) = \mathbf{0},$$

where we presumed $\overline{\Delta\alpha} = \Delta\alpha$ and $\overline{\Delta\beta} = \Delta\beta$. After the algebraic manipulations confined in Section 8.2, we conclude that

$$\Delta a = \frac{\mathbf{f}_C \cdot \mathbf{c}}{k_a} = f/k_a, \quad \Delta b = \frac{\mathbf{f}_B \cdot \mathbf{b}}{k_a} = -\frac{1}{2} \cos \alpha f/k_a = \frac{1}{4} f/k_a, \quad (27)$$

and

$$\begin{aligned} \Delta\alpha &= \frac{\sin \alpha}{4 \left(1 + 2 \frac{\tan^2 \beta/2}{\tan^2 \alpha}\right)} f s/k_s = \frac{3\sqrt{3}(1 + \cos \beta)}{8(5 + \cos \beta)} f s/k_s \\ \Delta\beta &= \frac{\cos \alpha \sin^2 \alpha \sin \beta}{3 - \cos \beta + \cos 2\alpha (1 - 3 \cos \beta)} f s/k_s = -\frac{3 \sin \beta}{4(5 + \cos \beta)} f s/k_s. \end{aligned} \quad (28)$$

4.3 Torsion of an ACNT

This problem has been dealt with in [15, 24]. The Euler cut in Figure 15 individuates a double ABU, a five-stick complex that we require to be in equilibrium under a system of forces and couples applied at points C, D, E , and F .

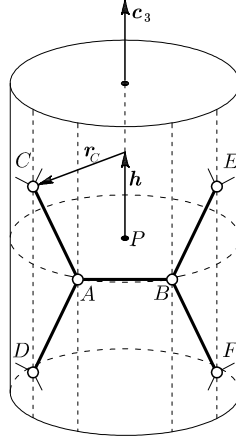


Figure 15: A double ABU and its adjacent sticks: front view.

As to forces, on guessing the problem's symmetries, we assume that

$$\begin{aligned} \mathbf{f}_C &= h\mathbf{t}_C + v\mathbf{c}_3, & \mathbf{f}_D &= -h\mathbf{t}_C + v\mathbf{c}_3, \\ \mathbf{f}_E &= h\mathbf{t}_E - v\mathbf{c}_3, & \mathbf{f}_F &= -h\mathbf{t}_E - v\mathbf{c}_3, \end{aligned} \quad (29)$$

with $\mathbf{t}_C, \mathbf{t}_E$ the unit vectors orthogonal to \mathbf{c}_3 and tangent at points C and E , respectively, to the cylinder on which all C atoms are sitting (see Figure 16); note that (29) implies that the resultant of this force system is null.

As to couples, we guess that angle changes are equal at points C and F and at points D and E :

$$\begin{aligned} \Delta\alpha(C) &= \Delta\alpha(F), & \Delta\beta(C) &= \Delta\beta(F); \\ \Delta\alpha(D) &= \Delta\alpha(E), & \Delta\beta(D) &= \Delta\beta(E). \end{aligned} \quad (30)$$

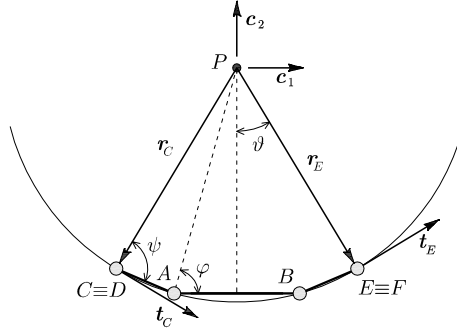


Figure 16: A double ABU: top-down view.

and that, moreover, angle changes are opposite at points C and D and at points E and F :

$$\begin{aligned}\Delta\alpha(C) &= -\Delta\alpha(D), & \Delta\beta(C) &= -\Delta\beta(D); \\ \Delta\alpha(E) &= -\Delta\alpha(F), & \Delta\beta(E) &= -\Delta\beta(F).\end{aligned}\quad (31)$$

Combining (30) and (31), we arrive at the following set of symmetry-based assumptions:

$$\begin{aligned}\Delta\alpha(C) &= \Delta\alpha(F) = -\Delta\alpha(E) = -\Delta\alpha(D), \\ \Delta\beta(C) &= \Delta\beta(F) = -\Delta\beta(E) = -\Delta\beta(D).\end{aligned}\quad (32)$$

The equilibrium of our stick complex is guaranteed if the resultant moment with respect to any chosen pole of the forces and couples applied at points C, D, E, F is null and if, moreover, both the force and couple system acting on stick AC and the force and couple system acting on stick AD have null resultant moment with respect to point A .

The moment balance for the double ABU yields the scalar condition:

$$(\rho_0 \sin \vartheta)v - (k_s \cos \gamma)\Delta\alpha(C) + \left(k_s \sin \frac{\alpha \cos 2\gamma}{2 \sin \beta}\right)\Delta\beta(C) = -(s \sin \frac{\alpha}{2} \cos \vartheta)h. \quad (33)$$

The moment balances for the AC and AD sticks furnish a symmetry condition that we had not been able to guess, namely,

$$\Delta\alpha(A) = 0, \quad (34)$$

and three scalar conditions: and

$$\begin{aligned}
k_s \frac{\sin \gamma}{\sin \beta} (\Delta\beta(C) + \Delta\beta^u(A)) &= -(s \sin(\gamma - \vartheta)) h, \\
\left(s \cos \frac{\alpha}{2} \sin \gamma \right) v - (k_s \sin \gamma) \Delta\alpha(C) + k_s \sin \frac{\alpha}{2} \frac{\sin 2\gamma}{\sin \beta} \Delta\beta(C) &= -\left(s \sin \frac{\alpha}{2} \sin \vartheta \right) h, \\
\left(s \cos \frac{\alpha}{2} \cos \gamma \right) v - (k_s \cos \gamma) \Delta\alpha(C) + k_s \sin \frac{\alpha}{2} \frac{\cos 2\gamma}{\sin \beta} \Delta\beta(C) + k_s \frac{\sin \frac{\alpha}{2}}{\sin \beta} \Delta\beta^u(A) \\
&= -\left(s \sin \frac{\alpha}{2} \cos \vartheta \right) h,
\end{aligned} \tag{35}$$

where $\Delta\beta^u(A)$ denotes the change in angle between the AC and AB sticks. The developments necessary to arrive at these equations can be found in Section 8.3. The solution of the system of (33) and (35) is:

$$\begin{aligned}
v &= -\sin \frac{\alpha}{2} \frac{\sin(\vartheta - \gamma)}{\sin \gamma} \xi h, \quad \text{with } \xi^{-1} := \cos \frac{\alpha}{2} \cos \gamma - \frac{\rho_0}{s} \sin \vartheta, \\
\Delta\alpha(C) &= \sin \frac{\alpha}{2} \left(\cos \frac{\alpha}{2} \cos \vartheta - \frac{\rho_0}{s} \frac{\sin^2 \vartheta}{\sin \gamma} \right) \xi h s / k_s, \\
\Delta\beta(C) &= 0, \\
\Delta\beta^u(A) &= \sin \beta \frac{\sin(\vartheta - \gamma)}{\sin \gamma} h s / k_s.
\end{aligned} \tag{36}$$

Note, in particular, (36)₃, another difficult-to-guess symmetry condition. Note also that it follows from the definition in (36), with the use of (2), (4), and (116), that $\xi = -2$. Thus, the first two of (36) can be written in the following simpler form:

$$\begin{aligned}
v &= 2 \sin \frac{\alpha}{2} \frac{\sin(\vartheta - \gamma)}{\sin \gamma} h, \\
\Delta\alpha(C) &= 2 \sin \alpha \frac{\sin(\vartheta - \gamma) + \sin \vartheta}{\sin \gamma} h s / k_s.
\end{aligned} \tag{37}$$

It follows from the first relations in (29), (115), and (36), that the axial force in the sticks AC and AD is:

$$\mathbf{f}_C \cdot \mathbf{c} =: N(AC) = -N(AD) = -\left(\cos \frac{\alpha}{2} \cos(\vartheta - \gamma) - 2 \sin^2 \frac{\alpha}{2} \frac{\sin(\vartheta - \gamma)}{\sin \gamma} \right) h;$$

thus, their axial deformation is:

$$\Delta b(AC) = -\Delta b(AD) = -\left(\cos \frac{\alpha}{2} \cos(\vartheta - \gamma) - 2 \sin^2 \frac{\alpha}{2} \frac{\sin(\vartheta - \gamma)}{\sin \gamma} \right) h / k_a. \tag{38}$$

Moreover, the axial force in stick AB turns out to be null, so therefore

$$\Delta a = 0.$$

4.4 Radial loading of an ACNT

Figure 17 features a top view of a double ABU subject to radial forces of common intensity p , a load condition that we later assimilate to the radial pressure problem for a cylindrical shell. The front view is the same as in Figure 15. We

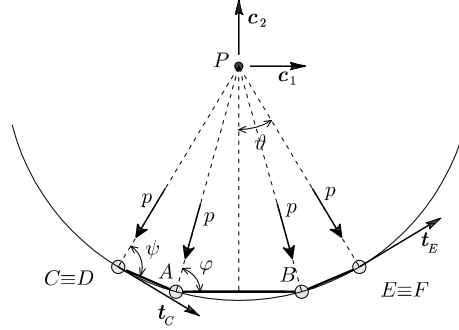


Figure 17: A double ABU subject to uniform radial forces: top-down view.

presume the following symmetries, for the applied forces consequential to our Euler cut:

$$\begin{aligned}
 \mathbf{f}_C &= \mathbf{f}_D, & \mathbf{f}_E &= \mathbf{f}_F, \\
 \mathbf{f}_C \cdot \mathbf{c}_1 &= -\mathbf{f}_E \cdot \mathbf{c}_1, \\
 \mathbf{f}_C \cdot \mathbf{c}_2 &= \mathbf{f}_E \cdot \mathbf{c}_2, \\
 \mathbf{f}_C \cdot \mathbf{c}_3 &= \mathbf{f}_E \cdot \mathbf{c}_3 = 0,
 \end{aligned} \tag{39}$$

and for the angle changes:

$$\Delta\alpha(A) = \Delta\alpha(C) =: \Delta\alpha, \quad \Delta\beta(A) = \Delta\beta(C) =: \Delta\beta, \tag{40}$$

where $\Delta\alpha, \Delta\beta$ satisfy (9).

Given (39), and given that

$$\mathbf{f}_A + \mathbf{f}_B = -2 \sin \varphi p \mathbf{c}_2,$$

the resultant of the force system is null if

$$-p \sin \varphi \mathbf{c}_2 + \mathbf{f}_C + \mathbf{f}_E = \mathbf{0},$$

i.e., if, in addition to the second of (39),

$$\mathbf{f}_C \cdot \mathbf{c}_2 = \frac{\sin \varphi}{2} p. \tag{41}$$

Only one more balance equation is needed, and we choose it to express the rotation equilibrium of stick AC with respect to point A :

$$\mathbf{p}_C \times \mathbf{f}_C + \boldsymbol{\tau}_\alpha + \boldsymbol{\tau}_\beta + \bar{\boldsymbol{\tau}}_\alpha + \bar{\boldsymbol{\tau}}_\beta = \mathbf{0}, \tag{42}$$

where, with the use of (40),

$$\begin{aligned}
\boldsymbol{\tau}_\alpha &= \tau_\alpha \mathbf{c} \times \mathbf{d}, & \tau_\alpha &= k_s \Delta\alpha |\mathbf{c} \times \mathbf{d}|^{-1}, \\
\boldsymbol{\tau}_\beta &= -\tau_\beta \mathbf{b} \times \mathbf{c}, & \tau_\beta &= k_s \Delta\beta |\mathbf{c} \times \mathbf{b}|^{-1}, \\
\bar{\boldsymbol{\tau}}_\alpha &= \bar{\tau}_\alpha (-\mathbf{e}) \times (-\mathbf{d}), & \bar{\tau}_\alpha &= k_s \Delta\alpha |\mathbf{c} \times \mathbf{d}|^{-1}, \\
\bar{\boldsymbol{\tau}}_\beta &= -\bar{\tau}_\beta \mathbf{e} \times (-\mathbf{c}), & \bar{\tau}_\beta &= k_s \Delta\beta |\mathbf{c} \times \mathbf{e}|^{-1}.
\end{aligned} \tag{43}$$

The algebraic manipulations in Section (8.4) allow us to conclude that

$$\Delta\alpha = -\frac{\sin \alpha \sin \varphi}{2 \left(4 \cos \frac{\alpha}{2} \sin \gamma + \widehat{\delta}^A(\alpha, \beta, \gamma) \sin \alpha \sin^{-1} \beta \sin 2\gamma \right)} ps/k_s, \tag{44}$$

where, we recall,

$$\widehat{\delta}^A(\alpha, \beta, \gamma) = \frac{\sin \frac{\alpha}{2}}{2 \sin \beta} \cos \gamma;$$

as to the axial deformation, we obtain:

$$\Delta a = \left(\widehat{\delta}^A(\alpha, \beta, \gamma) \sin \varphi \right) p/k_a, \tag{45}$$

and

$$\Delta b = \frac{1}{2} \left(\cos \frac{\alpha}{2} (\sin \gamma + \cot \gamma \cos \gamma) \sin \varphi \right) p/k_a. \tag{46}$$

4.5 Radial loading of a ZCNT

Consider a double ZBU, subject to applied radial forces of common intensity p (Figure 18), and imagine it isolated from the CNT it belongs to by means of an Euler cut.

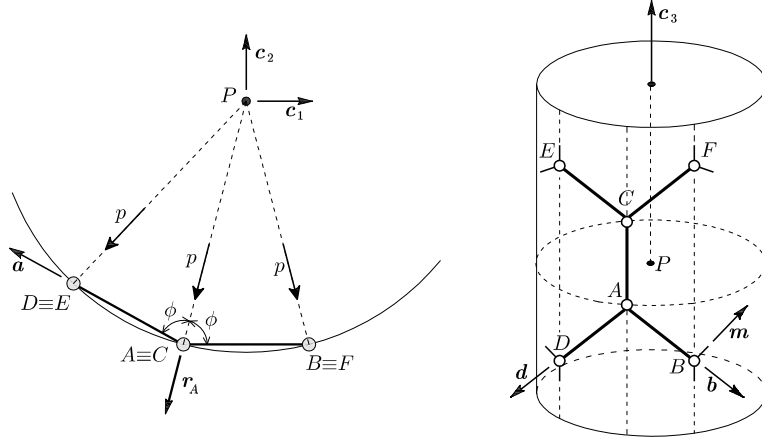


Figure 18: A double ZBU subject to uniform radial forces: top-down and front views.

We see that:

$$\mathbf{f}_C = \mathbf{f}_A = p \mathbf{r}_A, \quad \text{with} \quad \mathbf{r}_A := - \left(\sin \frac{\gamma}{2} \mathbf{c}_1 + \cos \frac{\gamma}{2} \mathbf{c}_2 \right) \quad (47)$$

(with reference to Figure 18-left, note that $\phi = (\pi - \gamma)/2$). The force symmetries we presume are:

$$\mathbf{f}_D = \mathbf{f}_E, \quad \mathbf{f}_B = \mathbf{f}_F, \quad \mathbf{f}_D \cdot \mathbf{r}_A = \mathbf{f}_B \cdot \mathbf{r}_A, \quad \mathbf{f}_D \cdot \mathbf{r}_A^\perp = -\mathbf{f}_B \cdot \mathbf{r}_A^\perp,$$

where $\mathbf{r}_A^\perp := \mathbf{r}_A \times \mathbf{c}_3$; in addition, we presume that

$$\mathbf{f}_D \cdot \mathbf{c}_3 = \mathbf{f}_B \cdot \mathbf{c}_3 = 0. \quad (48)$$

Under these presumptions, only two balance equations are needed for equilibrium: the resultant of all forces applied at points A, B, C, D, E , and D and the resultant moment with respect to A of all forces and couples acting on stick AB must both be null (see Subsection 4.5 of the Appendix).

In view of (47), (4.5), and (48), the force balance equation reads:

$$\mathbf{f}_B + \mathbf{f}_D + p \mathbf{r}_A = \mathbf{0},$$

and is equivalent to its only scalar consequence:

$$(\mathbf{f}_B + \mathbf{f}_D) \cdot \mathbf{r}_A + p = 0, \quad (49)$$

or rather,

$$\sin \frac{\gamma}{2} \mathbf{f}_B \cdot \mathbf{c}_1 + \cos \frac{\gamma}{2} \mathbf{f}_B \cdot \mathbf{c}_2 = \frac{1}{2} p. \quad (50)$$

The moment balance for stick AB reads:

$$\mathbf{p}_B \times \mathbf{f}_B + \boldsymbol{\tau}_\alpha + \boldsymbol{\tau}_\beta + \bar{\boldsymbol{\tau}}_\alpha + \bar{\boldsymbol{\tau}}_\beta = \mathbf{0}, \quad (51)$$

where,

$$\begin{aligned} \boldsymbol{\tau}_\alpha &= \tau_\alpha \mathbf{b} \times \mathbf{c}_3, & \tau_\alpha &= k_s \Delta\alpha |\mathbf{b} \times \mathbf{c}_3|^{-1}, \\ \boldsymbol{\tau}_\beta &= -\tau_\beta \mathbf{d} \times \mathbf{b}, & \tau_\beta &= k_s \Delta\beta |\mathbf{d} \times \mathbf{b}|^{-1}, \\ \bar{\boldsymbol{\tau}}_\alpha &= \bar{\tau}_\alpha \mathbf{b} \times \mathbf{c}_3, & \bar{\tau}_\alpha &= k_s \Delta\alpha |\mathbf{b} \times \mathbf{c}_3|^{-1}, \\ \bar{\boldsymbol{\tau}}_\beta &= -\bar{\tau}_\beta \mathbf{m} \times (-\mathbf{b}), & \bar{\tau}_\beta &= k_s \Delta\beta |\mathbf{d} \times \mathbf{b}|^{-1}. \end{aligned} \quad (52)$$

The developments leading to establishing that

$$\begin{cases} \Delta\alpha = - \frac{1}{4 \sin \frac{\gamma}{2} \left(2 - \frac{\hat{\delta}^Z(\alpha, \beta, \gamma)}{\sin \beta} (\sin \alpha \cos \gamma + \sin \alpha) \right)} \frac{ps}{k_s}, \\ \Delta\beta = \hat{\delta}^Z(\alpha, \beta, \gamma) \Delta\alpha, & \hat{\delta}^Z(\alpha, \beta, \gamma) = - \frac{\sqrt{3}}{2 \sin \beta} (1 + \cos \gamma), \end{cases} \quad (53)$$

$$\Delta a = 0,$$

and

$$\Delta b = \frac{\sin \alpha}{2 \sin \frac{\gamma}{2}} \frac{p}{k_a}, \quad (54)$$

are found in Section 8.5.

4.6 Energetics

The elastic energy stored in a deformation can be evaluated in a number of alternative ways. We find it convenient to do it with reference to bond units.

4.6.1 The energy stored in A- and Z- CNTs under axial traction

With reference to Figure 10, the total energy stored in an ABU turns out to be:

$$\begin{aligned} U_{Ax}^{ABU} &= \frac{1}{2}k_a \left((\Delta a)^2 + 2(\Delta b)^2 \right) + \frac{1}{2}k_s \left((\Delta\alpha)^2 + 2(\Delta\beta)^2 + 2 \times \frac{1}{2}(\Delta\alpha)^2 + 4 \times \frac{1}{2}(\Delta\beta)^2 \right) \\ &= k_a(\Delta b)^2 + k_s \left((\Delta\alpha)^2 + 2(\Delta\beta)^2 \right), \end{aligned} \quad (55)$$

where Δb is given by (23)₂ and $\Delta\alpha, \Delta\beta$ by (24); for a ZBU (Figure 11), we find:

$$\begin{aligned} U_{Ax}^{ZBU} &= \frac{1}{2}k_a \left((\Delta a)^2 + 2(\Delta b)^2 \right) + \frac{1}{2}k_s \left(2(\Delta\alpha)^2 + (\Delta\beta)^2 + 4 \times \frac{1}{2}(\Delta\alpha)^2 + 2 \times \frac{1}{2}(\Delta\beta)^2 \right) \\ &= \frac{1}{2}k_a \left((\Delta a)^2 + 2(\Delta b)^2 \right) + k_s \left(2(\Delta\alpha)^2 + (\Delta\beta)^2 \right), \end{aligned} \quad (56)$$

with $\Delta a, \Delta b$ given by (27) and $\Delta\alpha, \Delta\beta$ by (28). There are $4n$ ABUs and $2n$ ZBUs in a module, so that the energy stored per module is:

$$U_{Ax}^{AM} = 4n U_{Ax}^{ABU}, \quad U_{Ax}^{ZM} = 2n U_{Ax}^{ZBU}. \quad (57)$$

4.6.2 The energy stored in a twisted armchair CNT

In this instance, the energy stored in an ABU is:

$$\begin{aligned} U_{To}^{ABU} &= \frac{1}{2}k_a \left[(\Delta a)^2 + 2(\Delta b(C))^2 + 2(\Delta b(D))^2 \right] + \frac{1}{2}k_s \left[2(\Delta\alpha)^2 + 2(\Delta\beta^u(A))^2 + \right. \\ &\quad \left. + 2(\Delta\beta^d(A))^2 + (\Delta\alpha(C))^2 + (\Delta\alpha(D))^2 + (\Delta\beta(C))^2 + (\Delta\beta(D))^2 \right] = \\ &= 2k_a(\Delta b(AC))^2 + k_s \left[2(\Delta\beta^u(A))^2 + (\Delta\alpha(C))^2 \right], \end{aligned} \quad (58)$$

where $\Delta\beta^u(A)$ is given by (36)₄, $\Delta\alpha(C)$ by (37)₂, and $\Delta b(AC)$ by (38).

4.6.3 The energy stored in A- and Z- CNTs subject to radial loading

The energy stored in an ABU is:

$$U_{Rd}^{ABU} = \frac{1}{2}k_a \left((\Delta a)^2 + 2(\Delta b)^2 \right) + k_s (1 + 2(\tilde{\delta}^A(\alpha, \beta, \gamma))^2) (\Delta\alpha)^2, \quad (59)$$

where $\Delta a, \Delta b$, and $\Delta\alpha$, are given, respectively, by (45), (46), and (44). For a ZBU, the stored energy is:

$$U_{Rd}^{ZBU} = k_a(\Delta b)^2 + (2 + (\tilde{\delta}^Z(\alpha, \beta, \gamma))^2)k_s(\Delta\alpha)^2, \quad (60)$$

where Δb and $\Delta\alpha$ are given by, respectively, (54) and (53)₁.

4.7 Slenderness and thinness

We here discuss two important properties of a SWCNT, its slenderness and its thinness, within the context of DSM.

For N the number of C atoms at our disposal (say, the largest number of atoms we can treat in a numerical simulation), those atoms can be arranged in a nanotube consisting of $\text{int}(N/N_M)$ modules, where $\text{int}(\cdot)$ denotes the integer-part mapping. For l_M the length of a module, we have the following formula for the length L of the nanotube in question:

$$L \approx \text{int}(N/N_M) l_M = \begin{cases} 2\sqrt{3} \text{int}(N/8n) s & (\text{armchair}) \\ 3 \text{int}(N/4n) s & (\text{zigzag}) \end{cases}.$$

Consequently, that nanotube's *aspect ratio* – that is, its diameter/length ratio – is:

$$\frac{2\rho_0}{L} \approx \begin{cases} \frac{\sqrt{3}}{2\pi} \frac{n}{\text{int}(N/8n)} & (\text{armchair}) \\ \frac{1}{\sqrt{3}\pi} \frac{n}{\text{int}(N/4n)} & (\text{zigzag}) \end{cases}. \quad (61)$$

where use has been made of (2) and (10). Therefore, a nanotube is *slender* if, roughly speaking, $n^2 \ll N$. Consistently, when matching theoretical predictions with computational results, convenient simulations should concern arrays of some $N = 10^3 n^2$ atoms or more, as a glance to (61) indicates.

The chirality index n has to do not only with the slenderness of A- and Z-CNTs, but also with their *thinness*. A purely geometrical notion of thinness is easy to state within the framework of CSM: given a cylindrical shell of diameter $2(\rho_o + \varepsilon)$ and length $2l$, we term it *thin* if $\varepsilon/\rho_o \ll 1$, that is to say, if its thickness-to-diameter ratio is small.⁴ Thickness, however, is an ill-defined notion for CNTs, especially when they are single-wall. This is why, in our opinion, a purely geometrical discrete notion of thinness makes no sense for CNTs. Be it as it may, on recalling relation (22) between radius and chirality, we can estimate as follows the ‘geometrical thinness’ of a (n, m) -SWNT of arbitrary chirality and radius ρ_0 :

$$\frac{s}{2\widehat{\rho}_0(n, m)} = \frac{\pi}{n\sqrt{3(1 + m/n + (m/n)^2)}} = \begin{cases} \frac{\pi}{3} n^{-1} & (\text{armchair}) \\ \frac{\pi}{\sqrt{3}} n^{-1} & (\text{zigzag}) \end{cases}. \quad (62)$$

Thus, for an ACNT to be thin, the chirality index n must be larger than, say, 10 or more, a rather rare occurrence. We shall see in Section 6.3 that a more appropriate, not purely geometrical, notion of thinness does yield a decreasing, but less pronounced, dependence on n : *shells mimicking the mechanical behavior of SWCNTs are generally not thin!*

⁴See [22] for a discussion of the non-geometric ingredients that a notion of thinness may contain.

5 Nanoscopic CSM. A SWCNT-Oriented Shell Theory

In the majority of papers where CNTs are regarded macroscopically as shells, textbook theories induced from classic three-dimensional *isotropic* elasticity are used; consequently, the shell response is characterized in terms of two elastic moduli.⁵ On the basis of the DSM modeling at the nanoscale of armchair and zigzag CNTs we here use, we think it better to view all CNTs, be they single- or multi-wall and whatever their chirality, as *orthotropic* cylindrical shells whose midsurface has a tangent plane coinciding with the orthotropy plane, so that the shell geometry agrees point-wise with the geometry intrinsic to the chosen type of material response (see Fig. 19, where the three little cylinders suggest what

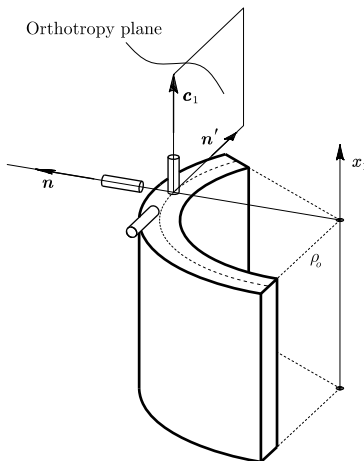


Figure 19: The geometrical elements relevant to describe the material response of CNTs modeled as shells.

probes one should cut out of the shell body in order to determine its material moduli). Such a shell theory has been fully developed in [8]; we here employ the simplest version fitting armchair and zigzag CNTs.

5.1 Displacement and strains

With reference to Fig. 20, given that $(x_1, \vartheta, \zeta) \in (-l, +l) \times (0, 2\pi) \times (-\varepsilon, +\varepsilon)$, the typical shell we consider as *length* $2l$, *wall thickness* 2ε , and *aspect ratio* ρ_o/l ; we call it *slender* if $\rho_o/l \ll 1$. In the theory we import from [8], displacement fields inducing thickness changes and thickness shearing are excluded a priori. In addition, for our present purposes, consideration of axisymmetric solutions to axisymmetric boundary value problems suffices. These solutions are

⁵There are, however, noticeable exceptions to this oversimplifying practice, such as [23] and [6].

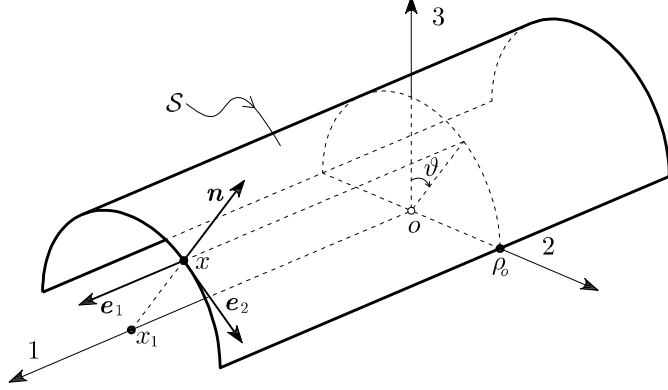


Figure 20: A portion of the model surface \mathcal{S} of a right cylindrical shell.

all independent of the circumferential coordinate ϑ , and have the following form in physical components $u_{\langle i \rangle}$:

$$u_{\langle 1 \rangle} = a_{\langle 1 \rangle} - \zeta w', \quad u_{\langle 2 \rangle} = \left(1 + \frac{\zeta}{\rho_o}\right) a_{\langle 2 \rangle}, \quad u_{\langle 3 \rangle} = w, \quad (63)$$

where a prime denotes differentiation with respect to x_1 , the only space variable from which all of the parameter fields $a_{\langle 1 \rangle}, a_{\langle 2 \rangle}$, and w , may depend. With the use of the linear strain measure

$$\mathbf{E}(\mathbf{u}) = \frac{1}{2}(\nabla \mathbf{u} + \nabla \mathbf{u}^T), \quad (64)$$

it is not difficult to see that

$$\mathbf{E}(\mathbf{u})\mathbf{n} = \mathbf{0},$$

i.e., that a shell of the type under study cannot change its thickness and that its fibers orthogonal to the referential midsurface \mathcal{S} must remain orthogonal to it after any admissible deformation. The not identically null strain components are:

$$\begin{aligned} E_{\langle 11 \rangle} &= a_{\langle 1 \rangle}' - \zeta w'', \\ E_{\langle 12 \rangle} &= \frac{1}{2} \left(1 + \frac{\zeta}{\rho_o}\right) a_{\langle 2 \rangle}', \\ E_{\langle 22 \rangle} &= \left(\rho_o \left(1 + \frac{\zeta}{\rho_o}\right)\right)^{-1} w \end{aligned} \quad (65)$$

(needless to say, $E_{\langle 12 \rangle} = E_{\langle 21 \rangle}$). On defining the *cross-section strain measure*:

$$\bar{\mathbf{E}}(x_1) := \frac{1}{2\varepsilon} \int_{-\varepsilon}^{+\varepsilon} \left(1 + \frac{\zeta}{\rho_o}\right) \mathbf{E}(x_1, \zeta), \quad (66)$$

we have from (65) that

$$\bar{E}_{\langle 11 \rangle} = a_{\langle 1 \rangle}', \quad \bar{E}_{\langle 12 \rangle} = \bar{E}_{\langle 21 \rangle} = \frac{1}{2} a_{\langle 2 \rangle}', \quad \bar{E}_{\langle 22 \rangle} = \rho_o^{-1} w. \quad (67)$$

5.2 Constitutive parameters

The mechanical response of the material comprising the cylindrical shells can be expressed in terms of five elastic moduli: $E_1, E_2, \nu_{12}, \nu_{21}, G$; the first two are Young-like moduli, the second two being Poisson-like, and the fifth being a shear modulus associated with the $(\mathbf{e}_1, \mathbf{e}_2)$ pair of directions; the first four are not independent, because it must be that

$$\frac{E_1}{E_2} = \frac{\nu_{12}}{\nu_{21}}. \quad (68)$$

5.3 Axisymmetric equilibria

Here below we record the equilibrium solutions of the axial traction, torsion, and pressure, problems; once again, the reader is referred to [8] for details.

5.3.1 Axial Traction

Suppose the only loading is a distribution of end tractions equivalent to two mutually balancing axial forces of magnitude

$$F = (2\pi\rho_o)p, \quad \text{with } p = O(\varepsilon). \quad (69)$$

One finds that $a_{<2>} \equiv 0$ and that, for a slender shell,

$$\begin{aligned} w(x_1) &= -\rho_o \nu_{12} \delta(\varepsilon/\rho_o) \frac{\varepsilon^{-1}p}{2E_1}, \\ a_{<1>}(x_1) &= (1 - \nu_{12}\nu_{21} (1 - \delta(\varepsilon/\rho_o))) \frac{\varepsilon^{-1}p}{2E_1} x_1, \end{aligned} \quad (70)$$

where

$$\delta(\varepsilon/\rho_o) := \frac{1 - \nu_{12}\nu_{21}}{\frac{1}{2\frac{\varepsilon}{\rho_o}} \log \frac{1+\frac{\varepsilon}{\rho_o}}{1-\frac{\varepsilon}{\rho_o}} - \nu_{12}\nu_{21}}; \quad (71)$$

note for later use that

$$\lim_{\varepsilon/\rho_o \rightarrow 0} \frac{1}{2\frac{\varepsilon}{\rho_o}} \log \frac{1+\frac{\varepsilon}{\rho_o}}{1-\frac{\varepsilon}{\rho_o}} = 1, \quad \text{whence} \quad \lim_{\varepsilon/\rho_o \rightarrow 0} \delta(\varepsilon/\rho_o) = 1.$$

5.3.2 Torsion

When the only applied load is a distribution of end tractions statically equivalent to two mutually balancing torques of magnitude

$$T = (2\pi\rho_o^2)t, \quad \text{with } t = O(\varepsilon), \quad (72)$$

the axial and radial displacements $a_{<1>}$ and w vanish identically, whereas

$$a_{<2>}(x_1) = \frac{1}{1 + \frac{\varepsilon^2}{\rho_o^2}} \frac{\varepsilon^{-1}t}{2G} x_1. \quad (73)$$

As shown in [8], these results hold for whatever the value of the aspect ratio.

5.3.3 Radial pressure

When the slender shell under study is subject to a uniform radial pressure $\varpi = O(\varepsilon)$, all the other applied loads being null, one again finds that $a_{\langle 2 \rangle} \equiv 0$. Moreover, for a slender shell,⁶

$$w(x_1) = \rho_o^2 \delta(\varepsilon/\rho_o) \frac{\varepsilon^{-1} \varpi}{2E_2} \quad \text{and} \quad a_{\langle 1 \rangle} = -\nu_{21} \delta(\varepsilon/\rho_o) \frac{\rho_o \varepsilon^{-1} \varpi}{2E_2} x_1. \quad (74)$$

6 The Effective Parameters of CNT-like Shells

No matter whether we model a SWCNT as a shell or as a stick-and-spring complex, we may regard it as a *cylindrical probe*. Two parameters characterize the mechanical response of a probe in an axial traction experiment, and one in torsion; their verbal definitions are, respectively,

$$s_{Ax} := \frac{\text{axial load}}{\text{axial deformation}}, \quad \nu_{Ax} := -\frac{\text{radial deformation}}{\text{axial deformation}}, \quad (75)$$

and

$$s_{To} = \frac{\text{axial torque}}{\text{axial twist}}; \quad (76)$$

s_{Ax} and s_{To} are stiffness measures, ν_{Ax} is a Poisson-like modulus of transverse contraction. Two additional parameters are needed to characterize the response of a SWCNT to radial loading, namely, the specific stiffness and Poisson-like moduli

$$s_{Rd} := \frac{\text{radial load}}{\text{radial deformation}}, \quad \nu_{Rd} := -\frac{\text{axial deformation}}{\text{radial deformation}}.$$

In this section we derive mathematical expressions for these five parameters within the frameworks of both continuous and discrete structure mechanics. The CSM expressions involve $E_1, E_2, \nu_{12}, \nu_{21}$, and G , the five elastic moduli of the shell theory we adopt, as well as two geometric parameters, ε and ρ_o , the shell's thickness and model-surface radius. The DSM expressions depend on the nanoscopic spring-stiffness moduli k_a and k_s , as well as on s , the C-C bond length, and ρ_0 , the radius of the cylinder on which the C atoms arrange themselves (both for A- and Z- CNTs, $\rho_0 \propto ns$, recall (2) and (10)). We aim to evaluate the constitutive and geometric parameters of our nanoscopically informed theory of CNT-like shells solely in terms of k_a, k_s, s , and n . Our simple method consists in equating as many as needed of the continuous and discrete expressions we derive in the next two subsections for the various stiffnesses and contraction moduli listed above.

⁶See [8] for a full treatment of the traction and pressure problems for shells of arbitrary aspect ratio.

6.1 ‘Continuous’ parameters

When we regard a slender cylindrical shell as a probe subject to an axial load F , we set:

$$s_{Ax}^{(c)} := \frac{F}{\overline{E}_{\langle 11 \rangle}} \quad \text{and} \quad \nu_{Ax}^{(c)} := -\frac{\overline{E}_{\langle 22 \rangle}}{\overline{E}_{\langle 11 \rangle}} \quad (77)$$

for the effective *axial stiffness* and *axial contraction modulus*. With the use of (67) and (70), we then find:

$$s_{Ax}^{(c)} = \frac{1}{1 - \nu_{12}\nu_{21}(1 - \delta(\varepsilon/\rho_o))} E_1 A(\varepsilon), \quad \nu_{Ax}^{(c)} = \frac{\delta(\varepsilon/\rho_o)}{1 - \nu_{12}\nu_{21}(1 - \delta(\varepsilon/\rho_o))} \nu_{12}, \quad (78)$$

where $A(\varepsilon) := 4\pi\rho_o\varepsilon$ is the area of the shell’s cross-section.

For a twisted shell of arbitrary slenderness, we set:

$$s_{T_o}^{(c)} := \frac{T}{\Theta}, \quad \Theta := \rho_o^{-1} a_{\langle 2 \rangle}, \quad (79)$$

where Θ denotes the change in cross-section rotation angle per unit length caused by the application of the axial torque T . Accordingly, with the use of (73), we find for the effective *torsional stiffness*:

$$s_{T_o}^{(c)} = GJ(\varepsilon), \quad J(\varepsilon) := 4\pi\rho_o^3\varepsilon \left(1 + \frac{\varepsilon^2}{\rho_o^2}\right)^{-1}, \quad (80)$$

where $J(\varepsilon)$ is the polar inertia moment of the cross section.⁷

In case of a uniform radial pressure ϖ , we define for our slender shell-like probe an effective *radial strain* $\rho_o^{-1}w$, in terms of which we set

$$s_{Rd}^{(c)} := \frac{\varpi}{\rho_o^{-1}w} \quad \text{and} \quad \nu_{Rd}^{(c)} := -\frac{E_{\langle 11 \rangle}}{\rho_o^{-1}w}$$

for, respectively, the effective *radial stiffness* and the effective *radial contraction modulus*. With these definitions, relations (74) yield:

$$s_{Rd}^{(c)} = \frac{2E_2\varepsilon/\rho_o}{\delta(\varepsilon/\rho_o)}, \quad \nu_{Rd}^{(c)} = \nu_{21}. \quad (81)$$

Remark. The dimensions of the stiffness parameters are:

$$\dim(s_{Ax}^{(c)}) = \text{force}, \quad \dim(s_{T_o}^{(c)}) = \text{force} \times (\text{length})^2, \quad \dim(s_{Rd}^{(c)}) = \text{force} \times (\text{length})^{-2}.$$

⁷Recall that (73), and hence (80), holds whatever the slenderness of the shell under consideration.

6.2 ‘Discrete’ parameters

On resuming the spring-and-stick models of an A- and a Z- CNT assembled in Section 3, we set:

$$s_{Ax}^{(d)} := \frac{F}{\Delta H^M / H^M} \quad \text{and} \quad \nu_{Ax}^{(d)} := -\frac{\Delta P^M / P^M}{\Delta H^M / H^M}, \quad (82)$$

for the discrete axial stiffness and axial contraction modulus, where H^M, P^M and $\Delta H^M, \Delta P^M$ are the undeformed height and perimeter of a module and their changes under the applied loads. While the first of these definitions parallels the first of (77) in a self-explanatory manner, the second one requires a motivation: ours is that, for n sufficiently large and axisymmetric loadings,

$$\Delta P^M / P^M \approx \Delta \rho_0 / \rho_0.$$

For an explicit evaluation of $s_{Ax}^{(d)}$ and $\nu_{Ax}^{(d)}$, we proceed case by case. We find (Appendix, Subsection 8.6):

- (armchair case)

$$s_{Ax}^{(d,A)} = \frac{4n}{\sqrt{3} + \frac{1}{4\sqrt{3}} \left(1 + \frac{3}{2 \tan^2 \beta}\right)^{-1} \frac{k_a s^2}{k_s}} k_a s \quad (83)$$

and

$$\nu_{Ax}^{(d,A)} = -\frac{1 - \frac{1}{4} \left(1 + \frac{3}{2 \tan^2 \beta}\right)^{-1} \frac{k_a s^2}{k_s}}{3 + \frac{1}{4} \left(1 + \frac{3}{2 \tan^2 \beta}\right)^{-1} \frac{k_a s^2}{k_s}} \quad (84)$$

- (zigzag case)

$$s_{Ax}^{(d,Z)} = \frac{n}{\frac{3}{4} + \frac{1}{8 \left(1 + \frac{3}{2} \frac{\cos^4(\gamma/2)}{\sin^2 \beta}\right)} \frac{k_a s^2}{k_s}} k_a s \quad (85)$$

and

$$\nu_{Ax}^{(d,Z)} = -\frac{\frac{1}{4} + \frac{\sqrt{3}(1+\cos \beta)}{8(5+\cos \beta)} \frac{k_a s^2}{k_s}}{\frac{3}{4} + \frac{1}{8 \left(1 + \frac{3}{2} \frac{\cos^4(\gamma/2)}{\sin^2 \beta}\right)} \frac{k_a s^2}{k_s}}. \quad (86)$$

An alternative way to evaluate discrete strains and stiffnesses is to make use of Lamé’s theorem of work and energy ([9], Section 28). As is well known, this theorem guarantees that, in a linearly elastic equilibrium problem, *the load work is twice the stored energy*. Accordingly, for axial traction,

$$F \Delta H^M = 2 U_{Ax}^M, \quad \text{with } U_{Ax}^M = \text{energy stored in a module.}$$

Hence, on applying definition (82)₁, we find:

$$s_{Ax}^{(d)} = \frac{F^2 H^M}{2 U_{Ax}^M};$$

in particular, when U^M is evaluated with the use of (55) and (57), (83) follows.

To estimate torsion stiffness, we invoke Lamé's theorem and write, for a module,

$$T\Theta H^M = 2U_{T_o}^M,$$

where T is the applied torque and Θ is the twist angle per unit of length; on inserting this relation in (80), we find:

$$s_{T_o}^{(d)} = \frac{T^2 H^M}{2U_{T_o}^M}.$$

For an ACNT, $T = 2n h \rho_0$, where h has been defined in Section 4.3 (see Fig. 15 and equations (29)). On using (2), (58), (36) and (37), we find:

$$s_{T_o}^{(d,A)} = \frac{9(\sqrt{3}/2\pi^2)n^3}{\cos(\gamma - \vartheta) + 2\frac{\sin^2(\gamma - \vartheta)}{\sin \gamma} + 2\left(2\frac{\sin^2 \beta \sin^2(\gamma - \vartheta)}{\sin^2 \gamma} + 3\left(\frac{1}{2}\cos \vartheta - \frac{\rho_0 \sin^2 \vartheta}{s \sin \gamma}\right)^2\right)\frac{k_a s^2}{k_s}} k_a s^3. \quad (87)$$

In the case of radial applied forces, the Lamé theorem yields:

$$N^M p w_{Rd} = 2U_{Rd}^M, \quad (88)$$

where w_{Rd} = radial displacement. It is the matter of a simple computation (Appendix, Subsection 6.2) to arrive at the following expressions for the discrete radial stiffnesses of a A- and Z- CNT:

$$s_{Rd}^{(d,A)} = \frac{32\frac{\sin^2 \gamma}{\sin^2 \varphi} n}{\sqrt{3}\pi \left(5 + 4 \cos 2\gamma + \frac{6}{8+3\frac{\cos^2 \gamma}{\sin^2 \beta}} \frac{k_a s^2}{k_s}\right)} k_a s^{-1}, \quad (89)$$

$$s_{Rd}^{(d,Z)} = \frac{16n(17 - 8 \cos 2\beta + 12 \cos \gamma + 3 \cos 2\gamma)\frac{\sin^2 \frac{\gamma}{2}}{\sin^2 \beta}}{3\pi \left(6 + 9\frac{\cos^4 \frac{\gamma}{2}}{\sin^2 \beta} + \frac{k_a s^2}{k_s}\right)} k_a s^{-1}, \quad (90)$$

likewise, it is not difficult to show that

$$\nu_{Rd}^{(d,A)} = \frac{3}{\sin^2 \beta} \frac{2\frac{k_a s^2}{k_s} - 11 + 2 \cos 2\beta(4 - \frac{k_a s^2}{k_s}) - 3 \cos 2\gamma}{4\left(3\frac{k_a s^2}{k_s} + 4\right) + 2 \cos \gamma \left(64 + 3 \cos \gamma \frac{1+8 \cos \gamma}{\sin^2 \beta}\right)}, \quad (91)$$

and

$$\nu_{Rd}^{(d,Z)} = -\frac{1}{3} + \frac{4}{3\left(1 + \frac{k_s}{k_a s^2} \left(6 + 9\frac{\cos^4 \frac{\gamma}{2}}{\sin^2 \beta}\right)\right)}. \quad (92)$$

6.3 Elastic moduli, thickness, and radius, of CNT-like shells

i. Contraction moduli. We choose the cylinder axis of a CNT-like shell parallel to the roll-up axis of an ACNT, and require that

$$\nu_{Rd}^{(c)} = \nu_{Rd}^{(d,A)}, \quad (93)$$

whence, by (81)₂ and (91), we obtain that

$$\nu_{21} = \frac{3}{\sin^2 \beta} \frac{2 \frac{k_a s^2}{k_s} - 11 + 2 \cos 2\beta \left(4 - \frac{k_a s^2}{k_s}\right) - 3 \cos 2\gamma}{4 \left(3 \frac{k_a s^2}{k_s} + 4\right) + 2 \cos \gamma \left(64 + 3 \cos \gamma \frac{1+8 \cos \gamma}{\sin^2 \beta}\right)}. \quad (94)$$

Likewise, on choosing the cylinder axis of a CNT-like shell made of the same orthotropic material parallel to the roll-up axis of a ZCNT, we get:

$$\nu_{12} = \nu_{Rd}^{(d,Z)} = -\frac{1}{3} + \frac{4}{3 \left(1 + \frac{k_s}{k_a s^2} \left(6 + 9 \frac{\cos^4 \frac{\gamma}{2}}{\sin^2 \beta}\right)\right)}. \quad (95)$$

The dependence of these two Poisson-like moduli on the size parameter n is shown in Figure 21; note that

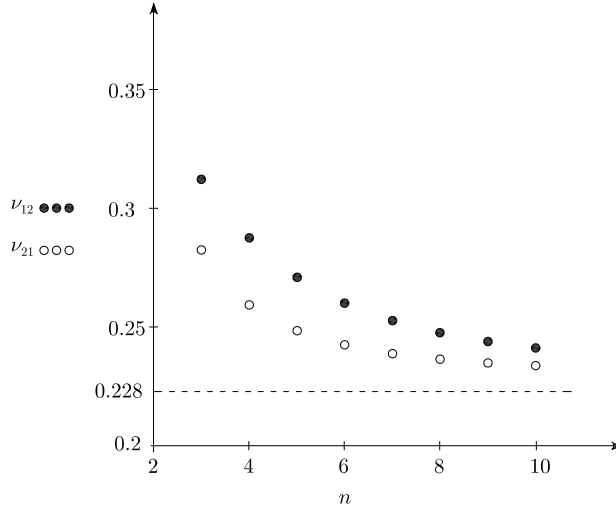


Figure 21: The contraction moduli ν_{21} (○) and ν_{12} (●) of ACNT-like shells.

$$\lim_{n \rightarrow \infty} \nu_{21} = \lim_{n \rightarrow \infty} \nu_{12} =: \nu^\infty = 0.228. \quad (96)$$

ii. Radius. With a view toward determining the *effective radii* ρ_o^A and ρ_o^Z of A- and Z- CNT-like shells, we observe that, by the use of (78)₁, (81)₁ and (78)₂,

and for (68) to hold, we find:

$$\frac{s_{Ax}^{(c)}}{s_{Rd}^{(c)}} = 2\pi\rho_o^2 \frac{\delta(\varepsilon/\rho_o)}{1 - \nu_{12}\nu_{21}(1 - \delta(\varepsilon/\rho_o))} \frac{E_1}{E_2} = 2\pi\rho_o^2 \frac{\nu_{Ax}^{(c)}}{\nu_{Rd}^{(c)}} \frac{E_1}{E_2} = 2\pi\rho_o^2 \frac{\nu_{Ax}^{(c)}}{\nu_{21}^{(c)}},$$

whence, thanks to (81)₂, we arrive at

$$\frac{s_{Ax}^{(c)}}{s_{Rd}^{(c)}} = 2\pi\rho_o^2 \frac{\nu_{Ax}^{(c)}}{\nu_{Rd}^{(c)}} \Leftrightarrow \rho_o = \sqrt{\frac{1}{2\pi} \frac{s_{Ax}^{(c)}}{s_{Rd}^{(c)}} \frac{\nu_{Rd}^{(c)}}{\nu_{Ax}^{(c)}}}.$$

We then set:

$$\rho_o^A := \sqrt{\frac{1}{2\pi} \frac{s_{Ax}^{(d,A)}}{s_{Rd}^{(d,A)}} \frac{\nu_{Rd}^{(d,A)}}{\nu_{Ax}^{(d,A)}}}, \quad \rho_o^Z := \sqrt{\frac{1}{2\pi} \frac{s_{Ax}^{(d,Z)}}{s_{Rd}^{(d,Z)}} \frac{\nu_{Rd}^{(d,Z)}}{\nu_{Ax}^{(d,Z)}}}. \quad (97)$$

Both effective radii depend on the size parameter n in a complex manner. But, as Fig. 22 shows, neither of them differs much, whatever n , from the corresponding

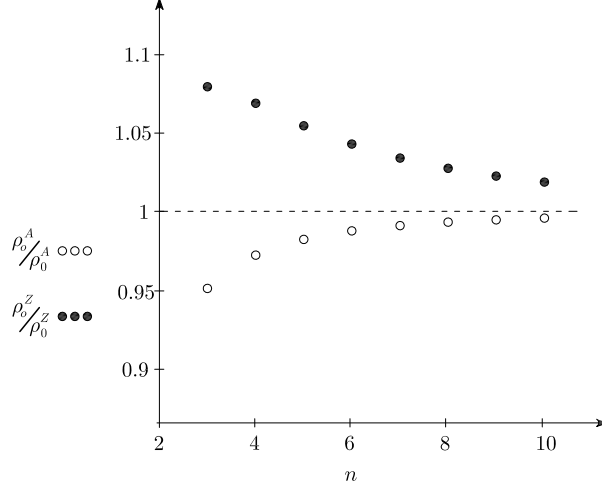


Figure 22: Ratio of effective and geometrically necessary radii of A-(○) and Z-(●) CNT-like shells.

value of the geometrically necessary radius; moreover, as n grows bigger they both tend to it:

$$\lim_{n \rightarrow \infty} \rho_o^A / \rho_0^A = \lim_{n \rightarrow \infty} \rho_o^Z / \rho_0^Z = 1.$$

iii. Thickness. We begin by laying down the following equality:

$$\frac{\delta(\varepsilon^A / \rho_o^A)}{1 - \nu_{12}\nu_{21}(1 - \delta(\varepsilon^A / \rho_o^A))} \nu_{12} = \nu_{Ax}^{(d,A)}, \quad (98)$$

where the values for ν_{21}, ν_{12} and ρ_o^A are chosen as agreed in i. and ii., and give it the role of an implicit equation that we solve for the unknown ε^A .⁸

As to ε^Z , we proceed as follows. Firstly, we equate the continuous and discrete radial stiffnesses of both A- and Z- CNTs:

$$\begin{aligned} 2E_2\varepsilon^A &= s_{Rd}^{(d,A)} \rho_o^A \delta(\varepsilon^A/\rho_o^A), \\ 2E_1\varepsilon^Z &= s_{Rd}^{(d,Z)} \rho_o^Z \delta(\varepsilon^Z/\rho_o^Z) \end{aligned} \quad (99)$$

(cf. (81)₁, (89), and (90)), whence, with the use of (68), we arrive at

$$\frac{\varepsilon^Z}{\varepsilon^A} = \frac{\nu_{21}}{\nu_{12}} \frac{s_{Rd}^{(d,Z)}}{s_{Rd}^{(d,A)}} \frac{\rho_o^Z}{\rho_o^A} \frac{\delta(\varepsilon^Z/\rho_o^Z)}{\delta(\varepsilon^A/\rho_o^A)}.$$

Finally, given that (98) implies that

$$\delta(\varepsilon^A/\rho_o^A) = \frac{\nu_{Ax}^{(d,A)}}{\nu_{12}} \frac{1 - \nu_{12}\nu_{21}}{1 - \nu_{21}\nu_{Ax}^{(d,A)}}, \quad (100)$$

and that a completely similar relation holds for $\delta(\varepsilon^Z/\rho_o^Z)$, we obtain:

$$\varepsilon^Z = \varepsilon^A \frac{s_{Rd}^{(d,Z)}}{s_{Rd}^{(d,A)}} \frac{\nu_{Ax}^{(d,Z)}}{\nu_{Ax}^{(d,A)}} \frac{1 - \nu_{21}\nu_{Ax}^{(d,A)}}{1 - \nu_{12}\nu_{Ax}^{(d,Z)}} \frac{\rho_o^Z}{\rho_o^A}. \quad (101)$$

Perusal of (98) and (101) yields for the effective thicknesses ε^A and ε^Z the dependences on the chirality index n shown in fig. 23.

iv. Extension moduli. Once effective radii and thicknesses have been computed, one way (there are others) to find the constitutive moduli E_1, E_2 is to combine (78) and (100), under the assumption that $s_{Ax}^{(c,A)} = s_{Ax}^{(d,A)}$ and $\nu_{Ax}^{(c,A)} = \nu_{Ax}^{(d,A)}$, so as to obtain:

$$E_1(2\varepsilon^A) = \frac{s_{Ax}^{(d,A)}}{2\pi\rho_o^A} \frac{1 - \nu_{12}\nu_{21}}{1 - \nu_{21}\nu_{Ax}^{(d,A)}}; \quad (102)$$

a germane relation holds for E_2 , namely,

$$E_2(2\varepsilon^Z) = \frac{s_{Ax}^{(d,Z)}}{2\pi\rho_o^Z} \frac{1 - \nu_{12}\nu_{21}}{1 - \nu_{21}\nu_{Ax}^{(d,Z)}}. \quad (103)$$

The dependence of both $E_1(2\varepsilon^A)$ and $E_2(2\varepsilon^Z)$ on n is shown in Figure 26; Figure 24 shows how the values of both E_1 and E_2 decay with n , their difference becoming smaller and smaller.

⁸With the use of (71), it is the matter of a short computation to give (98) the following form:

$$\frac{1}{2x} \log \frac{1+x}{1-x} = \frac{\nu_{21}}{\nu_{Ax}^{(d,A)}};$$

for \bar{x} the unique positive solution of this equation, we have that $\varepsilon^A = \rho_o^A \bar{x}$.

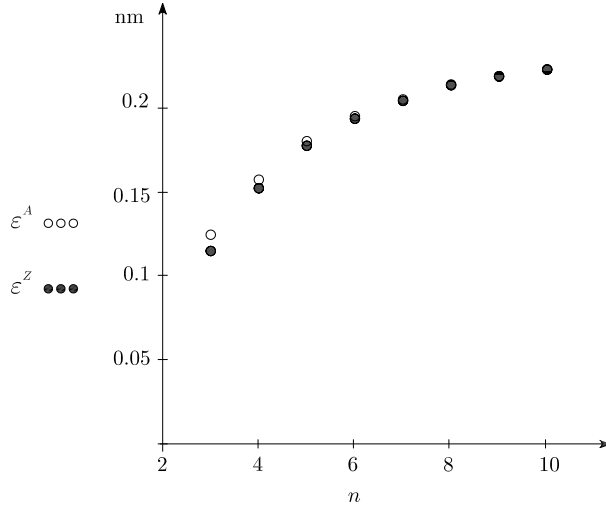


Figure 23: The effective thickness of A-(\circ) and Z-(\bullet) CNT-like shells.

v. Shear modulus. By equating the continuum and discrete evaluations (80) and (87) of the torsional stiffness, we find:

$$G = \frac{s_{T_o}^{(d)}}{J(\varepsilon)} = \frac{s_{T_o}^{(d)}}{4\pi(\rho_o^A)^3 \varepsilon^A} (1 + (\varepsilon^A/\rho_o^A)^2) \quad (104)$$

(see Figure 25).

vi. Consistency checks. The correctness of our computations can be checked in a number of ways. For one, (68), a key feature of our description of the constitutive response of orthotropic shell, is satisfied exactly, to all practical puposes, by the quadruplet $(E_1, E_2, \nu_{12}, \nu_{21})$ computed in the preceding subsections by equating continuous and discrete stiffnesses and contraction moduli. In fact, by an appropriate re-use of the computations made to construct Figures 21 and 24, one can show that, whatever the index n , $E_1/E_2 - \nu_{12}/\nu_{21} \approx 5 \times 10^{-16}$.

For two, the thickness ratio $\varepsilon^Z/\varepsilon^A$ can be evaluated in a way alternative to the one implicit in (23), namely,

$$\frac{\varepsilon^Z}{\varepsilon^A} = 2\pi\rho_o^A\rho_o^Z \frac{s_{Rd}^{(d,Z)}\nu_{Ax}^{(d,Z)}}{s_{Ax}^{(d,A)}\nu_{21}} \frac{1 - \nu_{21}\nu_{Ax}^{(d,A)}}{1 - \nu_{12}\nu_{Ax}^{(d,Z)}}, \quad (105)$$

with numerically identical results. Interestingly, no matter whether (23) or (105) is used, one has that

$$\lim_{n \rightarrow \infty} \frac{\varepsilon^Z}{\varepsilon^A} = 1,$$

that is to say, the thickness of A- and Z- CNTs of larger and larger radius tends to be the same.

⁹(105) is arrived at without presuming that (68) holds.

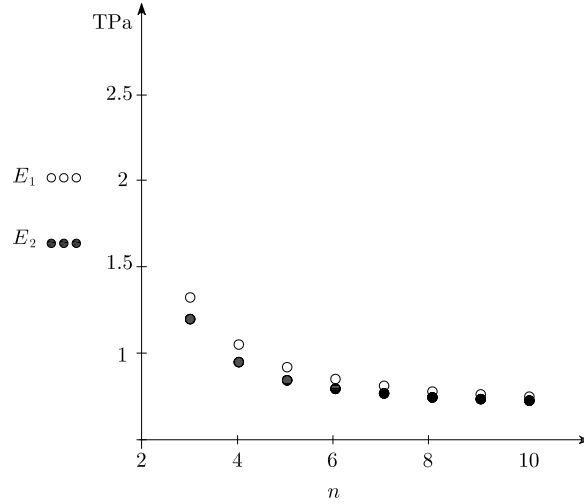


Figure 24: The extension moduli of CNT-like shells.

7 Conclusions

We have presented a procedure to determine the constitutive moduli and the geometric parameters to be associated with a single-wall carbon nanotube of given chirality in order to model it as a linearly elastic orthotropic cylindrical shell; our findings are summarized in the following table, for various values of the chirality index n , where we have set $h^A := 2\varepsilon^A$, $h^Z := 2\varepsilon^Z$.

n	6	10	20
E_1 (TPa)	0.832	0.736	0.709
E_2 (TPa)	0.784	0.729	0.706
ν_{12}	0.260	0.241	0.232
ν_{21}	0.242	0.233	0.230
G (TPa)	0.424	0.359	0.307
h^A (nm)	0.390	0.446	0.466
ρ_o^A (nm)	0.402	0.675	1.354

n	6	10	20
E_1 (TPa)	0.784	0.729	0.706
E_2 (TPa)	0.832	0.736	0.709
ν_{12}	0.242	0.233	0.230
ν_{21}	0.260	0.241	0.232
G (TPa)	0.424	0.359	0.307
h^Z (nm)	0.388	0.446	0.466
ρ_o^Z (nm)	0.245	0.399	0.787

Table 1. Elastic moduli, thickness and radius of CNT-like shells (A-, left; Z-, right).

As anticipated in our introductory section, the list of constitutive and geometric parameters appropriate for a SWCNT of arbitrary chirality pair (n, m) can be deduced for either one of the two lists in Table 1. A feature of our procedure is that each of these parameters, in addition to chirality, depends only on the two material constants modulating the harmonic approximations of the

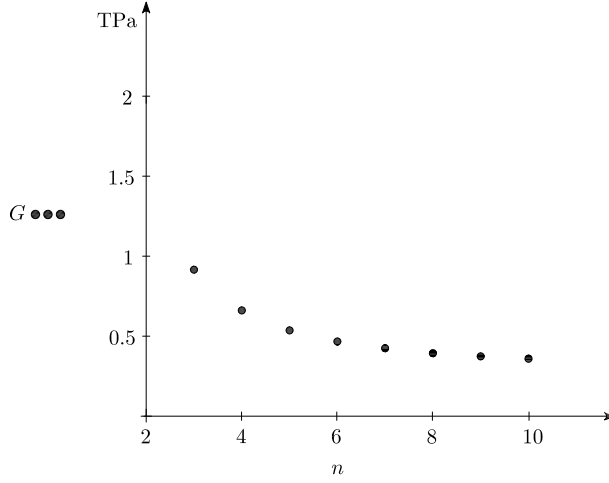


Figure 25: The shear modulus of ACNT-like shells.

nanoscopic bonding energies and on the length of a C-C bonds.¹⁰

Here is an interesting conclusion that can be drawn from our results in the so-called ‘graphene limit’, that is, for index $n \rightarrow \infty$. We have that

$$E_1/E_2 = \frac{\rho_o^A s_{Ax}^{(d,Z)} \varepsilon^A}{\rho_o^Z s_{Ax}^{(d,A)} \varepsilon^Z} \frac{1 - \nu_{12}\nu_{21}(1 - \delta(\varepsilon^A/\rho_o^A))}{1 - \nu_{12}\nu_{21}(1 - \delta(\varepsilon^Z/\rho_o^Z))} \rightarrow 1, \quad \nu_{12}/\nu_{21} \rightarrow 1, \quad h^A/h^Z \rightarrow 1;$$

moreover,

$$\begin{aligned} \lim_{n \rightarrow \infty} Gh^A &=: G^\infty h^\infty = 0.143 \text{ TPa} \times \text{nm}, \\ \lim_{n \rightarrow \infty} E_1 h^A &=: E^\infty h^\infty = 0.332 \text{ TPa} \times \text{nm}, \\ \nu^\infty &= 0.228 \end{aligned}$$

(recall (96)). Now, it is to check that

$$\frac{E^\infty h^\infty}{2(1 + \nu^\infty)} = 0.135 \text{ TPa} \times \text{nm} \neq G^\infty h^\infty,$$

whereas equality should hold when graphene, modeled within linear plane elasticity, is regarded as isotropic.

Another feature of our study is that it allows for determining in a mutually consistent manner the values of both wall thickness and Young modulus of a SWCNT. What value to take for thickness has been an issue in the nanotube community for long. Needless to say, an evaluation of effective thickness is necessary to apply any shell theory, ours being no exception. In the following

¹⁰These three nanoscopic bits of information can be put together under form of a dimensionless characteristic number, namely, $\frac{k_o s^2}{k_s} = 13.101$, measuring the relative importance of stretching and angle-changing energies.

table, a subset of Table 1 of [11], values for wall thickness and Young modulus of a SWCNT are listed, as determined by a number of different procedures; we have added a last column, for the values of the *tensile rigidity* [11], that is, the product Young’s modulus \times wall thickness.

Authors	Method	Wall thickness h (nm)	Young’s modulus E (TPa)	Tensile rigidity Eh (TPa \times nm)
Lu [17]	Molecular dynamics	0.34	0.974	0.331
Hernandez et al. [10]	Tight-binding molecular dynamics	0.34	1.24	0.422
Li and Chou [15]	Structural mechanics: stiffness matrix method	0.34	1.01	0.343
Jin and Yuan [13]	Molecular dynamics	0.34	1.238	0.421
Yakobson [30] et al.	Molecular dynamics	0.066	5.5	0.363
Zhou et al. [32]	Tight-binding model	0.074	5.1	0.377
Kudin et al. [14]	<i>Ab initio</i> computations	0.089	3.859	0.343
Tu and Ou-Yang [26]	Local density approximation model	0.075	4.7	0.352
Vodenitcharova and Zhang [27]	Ring theory continuum mechanics	0.0617	4.88	0.301
Pantano et al. [21]	Continuum shell modeling	0.075	4.84	0.363
Wang et al. [29]	<i>Ab initio</i> calculation	0.0665	5.07	0.337

Interestingly, while the reported values for wall thickness and Young modulus display a large scattering – the so-called *Yakobson’s paradox* [25] – the tensile rigidity has a very small variance, irrespectively of the method used to evaluate the factors. We regard this evidence as an implicit resolution of the paradox, in that it makes evident what one can sensibly try and evaluate: the stiffness parameters defined in Section 6, or others of the same sort, in two ways to be juxtaposed, discrete and continuous.

Note that the values furnished by our theory for the tensile rigidity comply with those in the table whatever the chirality index; Figure 26 summarizes our findings.

Finally, it is worth noticing that, in the light of our present theory, two notions of thinness can be given for a SWCNT. The first, *geometric thinness*, is expressed by formula (62); it depends exclusively on the chirality index n , by way of the ratio of the length s of the C-C bond and the geometrically necessary radius ρ_0 . The second, *effective thinness*, is ε/ρ_o ; here both ε and ρ_o depend in a complicated way, in addition to s and n , on the constitutive nanoscopic stiffness parameters k_a and k_s . Figure 27 shows that the effective thinness, while being greater than the geometric one, approaches zero as n grows in the same n^{-1} –way as the latter; it also shows that for small radii CNT-like shells are far from being thin.

8 Appendix. Ancillary Computations

8.1 Computations relative to Section 4.1

Note that

$$|\mathbf{b} \times \mathbf{c}| = \sin \beta = |\mathbf{c} \times \mathbf{e}|, \quad |\mathbf{c} \times \mathbf{d}| = \sin \alpha,$$

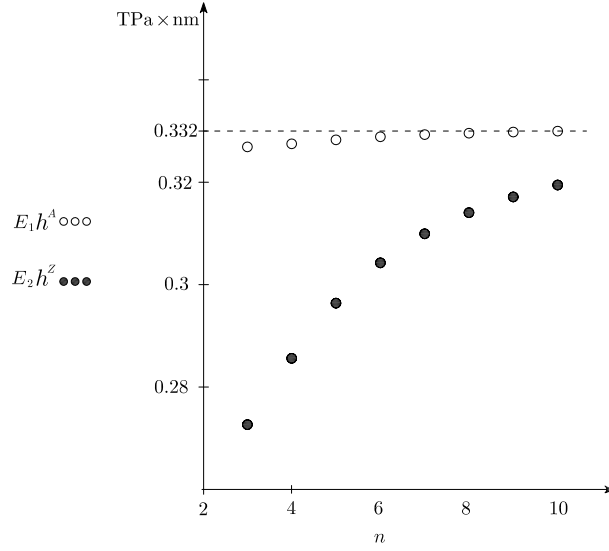


Figure 26: The tensile rigidity of A-(\circ) and Z-(\bullet) CNT-like shells.

two relations that will be useful to derive (106) here below. Combination with (17)₁, (18)-(21), and (22), allows us to give (20) the following form:

$$c \times (s f_C + 2\tau_\alpha d + \tau_\beta (e - b)) = 0; \quad (106)$$

thus, this equation has only two scalar counterparts. Now, with the use of (5)₂, (16), (17), and (22), one obtains:

$$c \times f_C = (f_C \cdot e_3) \cos \frac{\alpha}{2} \sin \gamma e_1 + \left((f_C \cdot e_3) \cos \frac{\alpha}{2} \cos \gamma - \frac{1}{2} (f_B \cdot e_1) \sin \frac{\alpha}{2} \right) e_2 + \frac{1}{2} (f_B \cdot e_1) \cos \frac{\alpha}{2} \sin \gamma e_3; \quad (107)$$

moreover, it follows from (5) and (7) that

$$\begin{aligned} c \times d &= -\sin \alpha (\sin \gamma e_1 + \cos \gamma e_2), \\ c \times e &= -\sin \frac{\alpha}{2} (\sin 2\gamma e_1 + \cos 2\gamma e_2) - \cos \frac{\alpha}{2} \sin \gamma e_3, \\ c \times b &= \sin \frac{\alpha}{2} e_2 - \cos \frac{\alpha}{2} \sin \gamma e_3. \end{aligned} \quad (108)$$

Consequently, in view also of (18), (19) and (21), the vector equation (106) yields the following scalar system:

$$\begin{cases} f_B \cdot e_1 = 0, \\ s \cos \frac{\alpha}{2} (f_C \cdot e_3) - 2k_s \left(\Delta\alpha - \Delta\beta \frac{\sin \frac{\alpha}{2}}{\sin \beta} \cos \gamma \right) = 0. \end{cases} \quad (109)$$

Thus, as to applied forces, we have:

$$f_B = 0, \quad f_C = -f_D = f e_3, \quad (110)$$

These developments lead to (23); (24) is arrived at by combining the second of (109) with (4)₁ and (9) and (110).

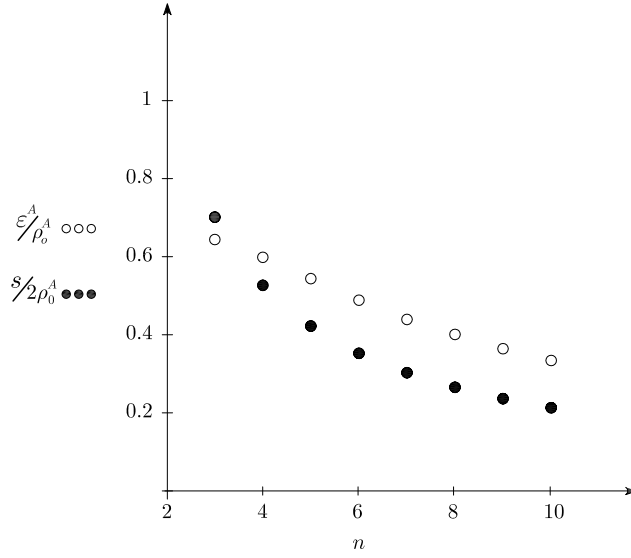


Figure 27: Geometric (●) and effective (○) thickness.

8.2 Computations relative to Section 4.2

On taking (12) into account, one finds that

$$s^{-1} \mathbf{p}_B \times \mathbf{f}_B = -(\mathbf{f}_B \cdot \mathbf{c}_2) \cos \alpha \mathbf{c}_1 + \left((\mathbf{f}_B \cdot \mathbf{c}_1) l \cos \alpha + \frac{1}{2} (\mathbf{f}_C \cdot \mathbf{c}_3) \sin \alpha \right) \mathbf{c}_2 + (\mathbf{f}_B \cdot \mathbf{c}_2) \sin \alpha \mathbf{c}_3;$$

moreover,

$$\begin{aligned} \mathbf{b} \times \mathbf{d} &= -\sin \alpha \cos \alpha \sin \gamma \mathbf{c}_1 - \sin \alpha \cos \alpha (1 + \cos \gamma) \mathbf{c}_2 + \sin^2 \alpha \sin \gamma \mathbf{c}_3, \\ \mathbf{b} \times \mathbf{m} &= -\sin \alpha \cos \alpha \sin \gamma \mathbf{c}_1 - (1 + \cos \gamma) \sin \alpha \sin \gamma \mathbf{c}_2 + \sin^2 \alpha \sin \gamma \mathbf{c}_3, \\ \mathbf{b} \times \mathbf{c}_3 &= -\sin \alpha \mathbf{c}_2. \end{aligned}$$

With the use of these relations, equation (26) yields the following scalar system:

$$\begin{cases} \mathbf{f}_B \cdot \mathbf{c}_2 = 0, \\ (\mathbf{f}_B \cdot \mathbf{c}_1) s \cos \alpha + \frac{1}{2} (\mathbf{f}_C \cdot \mathbf{c}_3) s \sin \alpha - 2k_s \frac{\Delta \beta}{\sin \beta} (1 + \cos \gamma) \sin \alpha \cos \alpha - 2k_s \Delta \alpha = 0. \end{cases} \quad (111)$$

Now, the first of (111) and the last of (25) imply that $\mathbf{f}_D \cdot \mathbf{a} \times \mathbf{c}_3 = 0$; with this and the penultimate of (25), the force balance (16) imply that $\mathbf{f}_B \cdot \mathbf{c}_1 = 0$. Summing up, the force system is:

$$\mathbf{f}_B = \mathbf{f}_D = -\mathbf{f}_C = -f \mathbf{c}_3,$$

whence the result in (27). Moreover, (111)₂ reduces to

$$\frac{1}{2} \frac{fs}{k_s} \sin \alpha - 2 \frac{\Delta \beta}{\sin \beta} (1 + \cos \gamma) \sin \alpha \cos \alpha - 2 \Delta \alpha = 0,$$

whence, with the use of (15), we obtain (28).

8.3 Computations relative to Section 4.3

(i) *Preparatory developments.* With a view toward formulating the equilibrium conditions for the AC and AD sticks, we supplement (32) with the following further guess:

$$\Delta\beta^u(A) = -\Delta\beta^d(A), \quad (112)$$

where $\Delta\beta^u$ ($\Delta\beta^d$) denotes the change in angle between the AC (AD) and AB sticks. Moreover, this time in preparation for formulating the first moment balance, we pick the pole P shown in Figure 15 and, with the help of Figure 16, we specify as follows the relative position vectors of the points where forces are applied:

$$\begin{aligned} \mathbf{p}_C &= \mathbf{h} + \mathbf{r}_C, & \mathbf{p}_D &= -\mathbf{h} + \mathbf{r}_C, \\ \mathbf{p}_E &= \mathbf{h} + \mathbf{r}_E, & \mathbf{p}_F &= -\mathbf{h} + \mathbf{r}_E, \end{aligned} \quad (113)$$

with

$$\begin{aligned} \mathbf{h} &= s \sin \frac{\alpha}{2} \mathbf{c}_3, \\ \mathbf{r}_C &= -\rho_0(\sin \vartheta \mathbf{c}_1 + \cos \vartheta \mathbf{c}_2) = \mathbf{r}_A + s \cos \frac{\alpha}{2} \mathbf{a}, \\ \mathbf{r}_E &= \rho_0(\sin \vartheta \mathbf{c}_1 - \cos \vartheta \mathbf{c}_2) = \mathbf{r}_B + s \cos \frac{\alpha}{2} \mathbf{a}', \\ \mathbf{r}_A &= -\rho_0(\cos \varphi \mathbf{c}_1 + \sin \varphi \mathbf{c}_2), & \mathbf{r}_B &= \rho_0(\cos \varphi \mathbf{c}_1 - \sin \varphi \mathbf{c}_2), \\ \mathbf{a} &= -\cos \gamma \mathbf{c}_1 + \sin \gamma \mathbf{c}_2, & \mathbf{a}' &= \cos \gamma \mathbf{c}_1 + \sin \gamma \mathbf{c}_2, \end{aligned} \quad (114)$$

and

$$\rho_0 = \frac{3}{2\pi} n s, \quad \varphi = \arccos \frac{\pi}{3n}, \quad \gamma = \frac{\pi}{2n}.$$

After some manipulations, we find:

$$\sin \vartheta = \cos \varphi + \frac{2\pi}{3n} \cos \frac{\alpha}{2} \cos \gamma, \quad \cos \vartheta = \sin \varphi - \frac{2\pi}{3n} \cos \frac{\alpha}{2} \sin \gamma,$$

whence

$$\mathbf{t}_C = \cos \vartheta \mathbf{c}_1 - \sin \vartheta \mathbf{c}_2, \quad \mathbf{t}_E = \cos \vartheta \mathbf{c}_1 + \sin \vartheta \mathbf{c}_2, \quad (115)$$

with

$$\vartheta = \widehat{\vartheta}(n) := \arcsin \left(\frac{\pi}{3n} \left(1 + \cos \frac{\pi}{2n} \right) \right); \quad (116)$$

we note here for later use that $\sin(\vartheta - \gamma) > 0$, for all $n \geq 2$.

(ii) *Moment balance for the double ABU.* The resultant moment of the force and couple system with respect to pole P reads:

$$\mathbf{m}_P + \overline{\mathbf{T}}_\alpha(C) + \overline{\mathbf{T}}_\beta(C) + \overline{\mathbf{T}}_\alpha(D) + \overline{\mathbf{T}}_\beta(D) + \overline{\mathbf{T}}_\alpha(E) + \overline{\mathbf{T}}_\beta(E) + \overline{\mathbf{T}}_\alpha(F) + \overline{\mathbf{T}}_\beta(F) = \mathbf{0}. \quad (117)$$

Here, \mathbf{m}_P is the moment of the force system with respect to pole P :

$$\mathbf{m}_P = \mathbf{p}_C \times \mathbf{f}_C + \mathbf{p}_D \times \mathbf{f}_D + \mathbf{p}_E \times \mathbf{f}_E + \mathbf{p}_F \times \mathbf{f}_F,$$

for which, with the use of (5), (29), and (113)-(115), we find:

$$\mathbf{m}_P = 4 \left(h s \sin \frac{\alpha}{2} \cos \vartheta + v \rho_0 \sin \vartheta \right) \mathbf{c}_2. \quad (118)$$

Moreover,

$$\begin{aligned} \overline{\mathbf{T}}_\alpha(C) &= \bar{\tau}_\alpha(C) (-\mathbf{c}) \times \mathbf{m}, & \bar{\tau}_\alpha(C) &= k_s \Delta\alpha(C) |\mathbf{c} \times \mathbf{m}|^{-1}, \\ \overline{\mathbf{T}}_\beta(C) &= -\bar{\tau}_\beta(C) \mathbf{e} \times (-\mathbf{c}), & \bar{\tau}_\beta(C) &= k_s \Delta\beta(C) |\mathbf{e} \times \mathbf{c}|^{-1}, \\ \overline{\mathbf{T}}_\alpha(D) &= -\bar{\tau}_\alpha(D) (-\mathbf{c}) \times \mathbf{m}, & \bar{\tau}_\alpha(D) &= k_s \Delta\alpha(D) |\mathbf{c} \times \mathbf{m}|^{-1}, \\ \overline{\mathbf{T}}_\beta(D) &= \bar{\tau}_\beta(D) (-\mathbf{d}) \times \mathbf{e}, & \bar{\tau}_\beta(D) &= k_s \Delta\beta(D) |\mathbf{d} \times \mathbf{e}|^{-1}, \\ \overline{\mathbf{T}}_\alpha(E) &= -\bar{\tau}_\alpha(E) \mathbf{m}' \times (-\mathbf{c}'), & \bar{\tau}_\alpha(E) &= k_s \Delta\alpha(E) |\mathbf{m}' \times \mathbf{c}'|^{-1}, \\ \overline{\mathbf{T}}_\beta(E) &= \bar{\tau}_\beta(E) (-\mathbf{c}') \times (\mathbf{e}'), & \bar{\tau}_\beta(E) &= k_s \Delta\beta(E) |\mathbf{c}' \times \mathbf{e}'|^{-1}, \\ \overline{\mathbf{T}}_\alpha(F) &= \bar{\tau}_\alpha(F) \mathbf{m}' \times (-\mathbf{c}'), & \bar{\tau}_\alpha(F) &= k_s \Delta\alpha(F) |\mathbf{m}' \times \mathbf{c}'|^{-1}, \\ \overline{\mathbf{T}}_\beta(F) &= -\bar{\tau}_\beta(F) (\mathbf{e}') \times (\mathbf{m}'), & \bar{\tau}_\beta(F) &= k_s \Delta\beta(F) |\mathbf{e}' \times \mathbf{m}'|^{-1}, \end{aligned} \quad (119)$$

where

$$\begin{aligned} e &= -\cos 2\gamma c_1 + \sin 2\gamma c_2, & e' &= \cos 2\gamma c_1 + \sin 2\gamma c_2; \\ c' &= \cos \frac{\alpha}{2} a' + \sin \frac{\alpha}{2} c_3, & d' &= \cos \frac{\alpha}{2} a' - \sin \frac{\alpha}{2} c_3; & m &= -d, & m' &= -d'. \end{aligned} \quad (120)$$

Making use of (118), (119) and (120), it is not difficult to see that, as a consequence of the symmetries embodied in (32), (117) is equivalent to the scalar equation (33)

(iii) *Moment balances for the AC and AD sticks.* For A the common pole, we request that

$$\begin{aligned} p_C \times f_C + \bar{\mathcal{T}}_\alpha(C) + \bar{\mathcal{T}}_\beta(C) + \mathcal{T}_\alpha(A) + \mathcal{T}_\beta^u(A) &= \mathbf{0}, \\ p_D \times f_D + \bar{\mathcal{T}}_\alpha(D) + \bar{\mathcal{T}}_\beta(D) - \mathcal{T}_\alpha(A) + \mathcal{T}_\beta^d(A) &= \mathbf{0}, \end{aligned} \quad (121)$$

where the terms not listed in (119) are defined as follows:

$$\begin{aligned} \mathcal{T}_\alpha(A) &= \tau_\alpha(A) c \times d, & \tau_\alpha(A) &= k_s \Delta\alpha(A) |c \times d|^{-1}, \\ \mathcal{T}_\beta^u(A) &= -\tau_\beta^u(A) b \times c, & \tau_\beta^u(A) &= k_s \Delta\beta^u(A) |b \times c|^{-1}, \\ \mathcal{T}_\beta^d(A) &= \tau_\beta^d(A) d \times b, & \tau_\beta^d(A) &= k_s \Delta\beta^d(A) |b \times d|^{-1}. \end{aligned} \quad (122)$$

Then, equations (121) can be rewritten as

$$\begin{aligned} c \times \left(s f_C + (\bar{\tau}_\alpha(C) + \tau_\alpha(A)) d - \bar{\tau}_\beta(C) e + \tau_\beta^u(A) b \right) &= \mathbf{0}, \\ d \times \left(s f_D + (\bar{\tau}_\alpha(D) - \tau_\alpha(A)) c - \bar{\tau}_\beta(D) e + \tau_\beta^d(A) b \right) &= \mathbf{0}. \end{aligned} \quad (123)$$

Note that $\Delta\alpha(A)$ is the fifth and last unknown in our equilibrium problem, the other four being v , $\Delta\alpha(C)$, $\Delta\beta(C)$, and $\Delta\beta^u$; the determining equations are (33) and the four scalar consequences of (123): by subtraction of one of (123) from the other, we find both (34) and (35)₁; by summation, we find (35)_{2,3}.

8.4 Computations relative to Section 4.4

Combining (42) and (43), we have:

$$c \times (s f_C + 2\tau_\alpha d + \tau_\beta b - \bar{\tau}_\beta e) = \mathbf{0},$$

an equation that, on recalling the definitions of the vectors involved, can be given the following form:

$$s f_C + 2\tau_\alpha d + \tau_\beta b - \bar{\tau}_\beta e = \lambda c, \quad \text{with } \lambda = -2\tau_\alpha,$$

or rather, equivalently,

$$s f_C + 2\tau_\alpha(c + d) + \tau_\beta b - \bar{\tau}_\beta e = \mathbf{0}. \quad (124)$$

The scalar consequences are two:

$$\begin{aligned} s(f_C \cdot c_1) - 4 \cos \frac{\alpha}{2} \cos \gamma \tau_\alpha + \tau_\beta + \cos 2\gamma \bar{\tau}_\beta &= 0, \\ s(f_C \cdot c_2) + 4 \cos \frac{\alpha}{2} \sin \gamma \tau_\alpha - \sin 2\gamma \bar{\tau}_\beta &= 0. \end{aligned}$$

If, in the second, we make use of (41) and (9), we find (44); with this, the first gives:

$$f_C \cdot c_1 = -\frac{1}{2} \cot \gamma \sin \varphi p. \quad (125)$$

As to axial forces and strains, in the a -type stick AB they are, respectively,

$$-2f_C \cdot b =: N(AB) = \cot \gamma \sin \varphi p, \quad (126)$$

whence we obtain (45); in all other b -type sticks they are:

$$f_C \cdot c := N(AC) = \frac{1}{2} \left(\cos \frac{\alpha}{2} (\sin \gamma + \cot \gamma \cos \gamma) \sin \varphi \right) p, \quad (127)$$

whence (46) follows.

8.5 Computations relative to Section 4.5

Combining (51) and (52), we have:

$$\mathbf{b} \times (s\mathbf{f}_B + 2\tau_\alpha \mathbf{c}_3 + \tau_\beta \mathbf{d} - \bar{\tau}_\beta \mathbf{m}) = \mathbf{0},$$

an equation equivalent to

$$s\mathbf{f}_B + 2\tau_\alpha (\mathbf{c}_3 + 2\mathbf{b}) + \tau_\beta (\mathbf{d} - \mathbf{m} - 2\mathbf{b}) = \mathbf{0},$$

whose two scalar consequences are:

$$\begin{cases} s(\mathbf{f}_B \cdot \mathbf{c}_1) + 4\tau_\alpha \sin \alpha - 2\tau_\beta (\sin \alpha \cos \gamma + \sin \alpha) = 0, \\ \mathbf{f}_B \cdot \mathbf{c}_2 = 0. \end{cases} \quad (128)$$

Equations (50) and (128)₂ allow to conclude that

$$\mathbf{f}_B \cdot \mathbf{c}_1 = \frac{1}{2 \sin \frac{\gamma}{2}} p.$$

With this, (128)₁, and (15), we obtain (53).

Finally, while it is obvious that $\Delta a = 0$, for Δb we have that

$$\Delta b = \frac{1}{k_a} \mathbf{f}_B \cdot \mathbf{b} = \frac{\sin \alpha}{2 \sin \frac{\gamma}{2}} \frac{p}{k_a}. \quad (129)$$

8.6 Computations relative to Section 6.2

To arrive at relations (83) and (84), one starts from

$$\begin{aligned} F &= 2n f \\ H^{AM} &= 4b \sin \frac{\alpha}{2}, \quad P^{AM} = 2n \left(a + b \cos \frac{\alpha}{2} \right), \\ \Delta H^{AM} &= 4 \sin \frac{\alpha}{2} \Delta b + 2b \cos \frac{\alpha}{2} \Delta \alpha, \quad \Delta P^{AM} = 2n \left(\Delta a + \cos \frac{\alpha}{2} \Delta b - \frac{1}{2} b \sin \frac{\alpha}{2} \Delta \alpha \right) \end{aligned}$$

(here, a, b denote the common undeformed length of sticks of type a and b , respectively), whence

$$\begin{aligned} \frac{\Delta H^{AM}}{H^{AM}} &= \frac{1}{2\sqrt{3}} \left(3 + \frac{1}{4} \left(1 + \frac{3}{2 \tan^2 \beta} \right)^{-1} \frac{k_a s^2}{k_s} \right) \frac{f}{k_a s}, \\ \frac{\Delta P^{AM}}{P^{AM}} &= \frac{1}{2\sqrt{3}} \left(1 - \frac{1}{4} \left(1 + \frac{3}{2 \tan^2 \beta} \right)^{-1} \frac{k_a s^2}{k_s} \right) \frac{f}{k_a s}. \end{aligned}$$

Quite similarly, equations (85) and (86) are arrived at on setting:

$$\begin{aligned} F &= n f \\ H^{ZM} &= 2(a - b \cos \alpha), \quad P^{ZM} = 2n b \sin \alpha, \\ \Delta H^{ZM} &= 2(\Delta a - \cos \alpha \Delta b + b \sin \alpha \Delta \alpha), \quad \Delta P^{ZM} = 2n(\sin \alpha \Delta b + b \cos \alpha \Delta \alpha), \end{aligned}$$

whence

$$\begin{aligned} \frac{\Delta H^{ZM}}{H^{ZM}} &= \left(\frac{3}{4} + \frac{3(1 + \cos \beta)}{8(5 + \cos \beta)} \frac{k_a s^2}{k_s} \right) \frac{f}{k_a s}, \\ \frac{\Delta P^{ZM}}{P^{ZM}} &= \left(\frac{1}{4} + \frac{\sqrt{3}(1 + \cos \beta)}{8(5 + \cos \beta)} \frac{k_a s^2}{k_s} \right) \frac{f}{k_a s}. \end{aligned}$$

* * * * *

It follows from (88) that

$$w_{Rd}^A = 2p^{-1}U_{Rd}^{ABU},$$

where U_{Rd}^{ABU} is deducible from (58) by using (45) and (46):

$$U_{Rd}^{ABU} = \frac{p^2}{16k_a} \frac{\sin^2 \varphi}{\sin^2 \gamma} \left(5 + 4 \cos 2\gamma + \frac{6}{8 + 3 \left(\frac{\cos \gamma}{\sin \beta} \right)^2} \frac{k_a s^2}{k_s} \right).$$

Thus,

$$w_{Rd}^A = \frac{p}{8k_a} \frac{\sin^2 \varphi}{\sin^2 \gamma} \left(5 + 4 \cos 2\gamma + \frac{6}{8 + 3 \left(\frac{\cos \gamma}{\sin \beta} \right)^2} \frac{k_a s^2}{k_s} \right).$$

References

- [1] X. Blanc, C. Le Bris, P.L. Lions, From Molecular Models to Continuum Mechanics, *Archive Rational Mech. Anal.*, 164, 4, 341:381, (2002).
- [2] G.X. Cao, X. Chen, The effects of chirality and boundary conditions on the mechanical properties of single-walled carbon nanotubes, *Int. J. Solids Struct.*, 44, 5447-5465 (2007).
- [3] T.C. Chang, Torsional behavior of chiral singlewalled carbon nanotubes is loading direction dependent, *Appl. Phys. Lett.*, 90, 201910 (2007).
- [4] T. Chang, H. Gao, Size-dependent elastic properties of a single nanotube via a molecular mode, *J. Mech. Phys. Solids*, 51:1059 (2003).
- [5] J. Geng, T. Chang, Nonlinear stick-spiral model for predicting mechanical behavior of single-walled carbon nanotubes, *Phys. Rev. B*, 74:245428 (2006).
- [6] R.V. Goldstein, V.A. Gorodtsov, A.V. Chentsov, S.V. Starikov, V.V. Stegailov, G.E. Norman, To description of mechanical properties of nanotubes. Tube wall thickness problem. Size effect, Russian Academy of Sciences, A.Yu. Ishlinsky Institute for Problems in Mechanics, Preprint 937 (2010).
- [7] R.V. Goldstein, V.A. Gorodtsov, D.S. Lisovenko, To the description of multilayer nanotubes in models of cylindrically anisotropic elasticity., *Phys. Mech.* 13 (1-2), (2010).
- [8] A. Favata, P. Podio-Guidugli, A new CNT-oriented shell theory, submitted (2011).
- [9] M.E. Gurtin, The Linear Theory of Elasticity. Pp. 1-295 of *Handbuch der Physik VIa/2*, Springer (1972).
- [10] E. Hernandez, C. Goze, P. Bernier, A. Rubio, Elastic Properties of C and BxCyNz Composite Nanotubes, *Phys. Rev. Lett.* 80, 4502 (1998)
- [11] Y. Huang, J. Wu, K.C. Hwang, Thickness of graphene and single-wall carbon nanotubes, *Phys. Rev. B*, 74, 245413 (2006).

- [12] S. Iijima, *Nature*, 354, 56 (1991).
- [13] Y. Jin and F.G. Yuan, Simulation of Elastic Properties of Single-Walled Carbon Nanotubes, *Compos. Sci. Technol.*, Vol. 63, pp. 1507-1515 (2003).
- [14] K.N. Kudin, G.E. Scuseria, and B.I. Yakobson C2F, BN and C nano-shell elasticity by ab initio computations. *Phys. Rev. B*, 64: 235406/10 (2001).
- [15] C. Li, T.-W. Chou, A structural mechanics approach for the analysis of carbon nanotubes, *Int. J. Solids Struct.*, 40:2487 (2003).
- [16] C. Le Bris, P. L. Lions, From atoms to crystals: a mathematical journey, *Bull. Amer. Math. Soc.*, 42, 291:363 (2005).
- [17] J.P. Lu, Elastic Properties of Carbon Nanotubes and Nanoropes, *Phys. Rev. Lett.* 79, 1297 (1997).
- [18] P.G. Martinsson, I. Babuška, Mechanics of materials with periodic truss or frame micro-structures, *Arch. Rational Mech. Anal.*, 185, 201:234, (2007).
- [19] G.M. Odegard, Modeling of Carbon Nanotube/Polymer Composites. In *Nanoengineering of Structural, Functional and Smart Materials*, eds. M.J. Schulz, A. Kelkar, M.J. Sundaresan, CRC Press (2005).
- [20] G.M. Odegard, Equivalent-Continuum Modeling of Nanostructured Materials. In *Handbook of Theoretical and Computational Nanotechnology*, eds. M. Rieth and W. Schommers, American Scientific Publishers (2006).
- [21] A. Pantano, D.M. Parks, M.C. Boyce, Mechanics of deformation of single- and multi-wall carbon nanotubes. *J. Mech. Phys. Solids*. 52(4), 789-821 (2004)
- [22] P. Podio-Guidugli, On structure thinness, mechanical and variational, pp. 227-242 of *Variational Formulations in Mechanics: Theory and Applications*, E. Taroco, E.A. de Souza Neto, and A.A. Novotny (Ed.s), CIMNE, 2007.
- [23] C.Q. Ru, Chirality-Dependent Mechanical Behavior of Carbon Nanotubes Based on an Anisotropic Elastic Shell Model, *Math. Mech. Sol.*, 14, 88-101 (2009).
- [24] L. Shen, J. Li, Transversely isotropic properties of single-walled carbon nanotube, *Phys. Rev. B* 69:045414 (2004).
- [25] O.A. Shenderova, V.V. Zhirnov, D.W. Brenner, Carbon Nanostructures. *Crit. Rev. Solid State Mater. Sci.* 27, 227-356 (2002).
- [26] Z.C. Tu and Z.C. Ou-Yang, Single-walled and multiwalled carbon nanotubes viewed as elastic tubes with the effective Young's moduli dependent on layer number, *Phys. Rev. B* 65, 233407 (2002).
- [27] T. Vodenitcharova and L. C. Zhang, Effective wall thickness of a single-walled carbon nanotube, *Phys. Rev. B* 68, 165401 (2003).

- [28] H. Wan and F. Delale, A structural mechanics approach for predicting the mechanical properties of carbon nanotubes. *Meccanica* 45: 4351 (2010).
- [29] L. Wang, Q. Zheng, J.Z. Liu and Q. Jiang, Size dependence of the thin-shell model for carbon nanotubes, *Phys. Rev. Lett.* 95, pp. 8297-8312 (2005).
- [30] B.I. Yakobson, C.J. Brabec, J. Bernholc, Nanomechanics of carbon tubes: instabilities beyond linear regime, *Phys. Rev. Lett.* 76, 2511 (1996).
- [31] Y.Y. Zhang, V.B. Tan. C.M. Wang Effect of chirality on buckling behavior of singlewalled carbon nanotubes, *Jour. Appl. Phys.*, 100, 074304 (2006).
- [32] X. Zhou, J.J. Zhou and Z.C. Ou-yang, Strain energy and Young's modulus of single-wall carbon nanotubes calculated from electronic energy-band theory, *Phys. Rev. B* 62, pp. 13692-13696 (2000).